β_3 subunit of integrin.[3] We found that platelet dense granule secretion was regulated by the small guanosine triphosphate (GTP)-binding protein Rab27.[4] Furthermore, we found a Rab27 effector protein, Munc13-4.[4] A defect in Munc13-4 has been reported to cause familial hemophagocytic lymphohistiocytosis.[5] In collaboration with the pediatric hematologist group, we characterized 35 Japanese patients wth hemophagocytic lymphohistiocytosis and found that 30% of these cases were caused by a defect in Munc13-4.[6]

Here, we summarize the results of Rab27-Munc13-4 axis in platelet granule secretion, presented in the Japanese Geriatric Society Meeting (2005).

Granule secretion assay using permeabilized platelets

Platelet dense granules contain adenosine diphosphate (ADP) and serotonin that are self-agonists and function in a positive feedback activation of platelets upon secretion. The assay methods are described in detail elsewhere.[7] Briefly, freshly obtained washed platelets were incubated with [^{3}H]serotonin to allow uptake into dense granules. After washing the platelets, the platelet plasma membrane was permeabilized with 0.6 μg/mL SLO. Usually, the permeabilized platelets per assay contained approximately 20 000 c.p.m. of [^{3}H]serotonin. The permeabilized platelets were incubated with an adenosine tri-phosphate (ATP) regeneration system and human platelet cytosol at 4°C for 30 min, followed by further incubation at 30°C for 2 min. Finally, the platelets were stimulated with 20 μmol/L Ca^{2+} by addition of $CaCl_2$ at 30°C for 1 min, and the reaction was stopped with ice cold stopping buffer. After removing the platelets by centrifugation, aliquots of the supernatant containing secreted [^{3}H]serotonin were measured by a liquid scintillation counter. The establishment of the assay enabled us to investigate the mechanism of the secretion using molecular biological and biochemical methods.

Small GTPase Rab27 regulates dense granule secretion in platelets

Rab GTPases are localized to their specific organelles and regulate several steps of vesicle transport including vesicle formation, vesicle traffic along cytoskeletal tracks and vesicle tethering to the target membrane (Fig. 1).[8] Rab GTPases are geranylgeranylated at their C-termini, and this post-translational modification is required for their membrane association and exertion of their functions. The guanosine diphosphate (GDP)-bound form is an inactive form and the GTP-bound form is an active form which interacts with its effector molecules to exert the functions. Conversion from the GTP-bound form into the GDP-bound form is mediated by intrinsic GTPase activity, which is stimulated by GTPase activating protein (GAP). Conversion of the GDP-bound form into the GTP-bound form is mediated by GDP/GTP exchange reaction, which is performed by the function of GDP/GTP exchange factor (GEF). RabGTPases have a unique negative regulator named Rab GDP dissociation inhibitor (GDI). RabGDI is a cytosolic protein, which forms a complex with GDP-bound forms of RabGTPases to inhibit the GDP/GTP exchange, and extracts RabGTPases from the membrane into cytosol.

In Rab27A defective *ashen* mice, the bleeding time has been shown to be prolonged presumably due to platelet dysfunction caused by a lack of intact dense granules in the platelets.[8] However, one report has shown that platelets of *ashen* mice are normal because Rab27B, a homolog of Rab27A with 71% identity at amino acid level, is also present in platelets and could substitute for the defect of Rab27A. Further examination would be required to conclude that Rab27A is involved in the biogenesis of the dense granules. On the other hand, it has not been addressed whether Rab27 is involved in the regulation of dense granule secretion in platelets once the granules are normally generated. We investigated whether Rab27 functions regulated the granule secretion using the semi-intact assay system.[4]

Small GTPases produced in *Escherichia coli* are not modified by the addition of prenyl groups at their C termini, which is essential for their correct localization and function. Incubation of permeabilized platelets with Rab27A and Rab27B purified from *E. coli* inhibited the Ca^{2+}-induced dense granule secretion in a concentration-dependent manner. Incubation of permeabilized platelets with other small GTPases such as Rab3B, Rab4B, Rab5A, or Rap1B, a Ras family small GTPase whose GTP-bound form has been shown to be increased upon platelet activation, had no effect indicating that the effect of Rab27 was specific. We prepared and purified mutant Rab27A-T23N, which preferentially binds GDP, and Rab27A-Q78L, which lacks GTPase activity. Incubation of permeabilized platelets with Rab27A-Q78L, but not Rab27A-T23N, inhibited the secretion in a concentration-dependent manner. Inhibition by unprenylated Rab27A-Q78L, wild type Rab27A, and Rab27B could be due to sequestration of putative Rab27 effector molecules from endogenous membrane-associated GTP-Rab27 by forming non-functional complexes with effector proteins (Fig. 2). Thus, we concluded that Rab27 is involved in the regulation of dense core granule secretion in platelets.

Identification of a Rab27-effector Munc13-4 and its functions

To elucidate the mechanism of Rab27, we attempted to identify GTP-Rab27-binding proteins that might mediate the function of Rab27 in the granule secretion from platelet cytosol by affinity chromatography. We

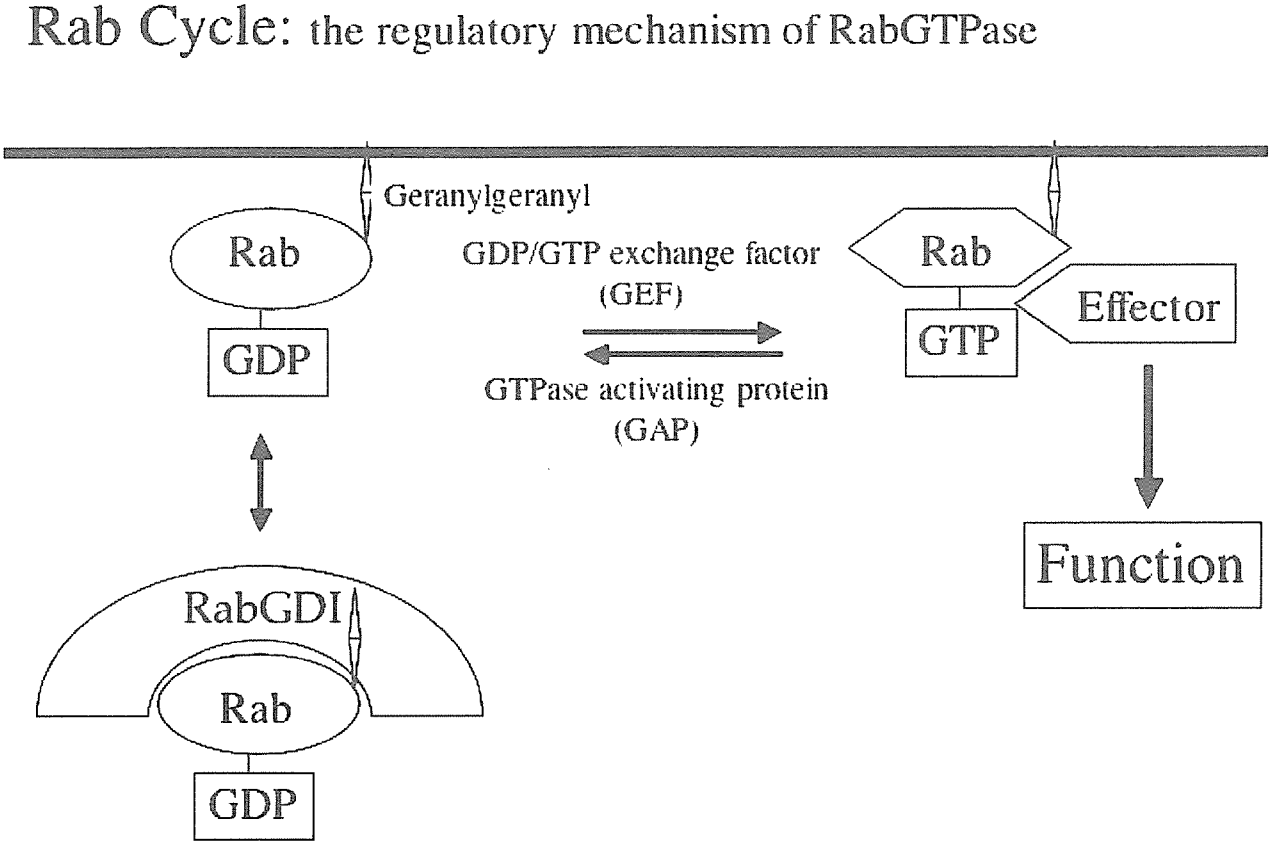

Figure 1 The Rab cycle. Rab GTPases are geranylgeranylated at their C-termini and bind to their correct organelle membrane. The activity of a Rab protein is regulated by bound nucleotide, GTP or GDP. The GDP-bound form is an inactive form and the GTP-bound form is an active form that interacts with its effector molecules to exert the functions. Conversion from the GTP-bound form into GDP-bound form is mediated by intrinsic GTPase activity, which is stimulated by the GTPase activating protein (GAP). Conversion of the GDP-bound form into the GTP-bound form is mediated by GDP/GTP exchange reaction, which is performed by the function of GDP/GTP exchange factor (GEF). Rab GTPases have a unique negative regulator named Rab GDP dissociation inhibitor (GDI). Rab GDI is a cytosolic protein, which forms a complex with GDP-bound forms of Rab GTPases to inhibit the GDP/GTP exchange, and extracts Rab GTPases from the membrane into cytosol.

identified a 120 kDa protein as human Munc13-4 by matrix-assisted laser desorption ionization time of flight mass spectrometry (MALDI TOF MS) analysis.[4] Using recombinant Rab27 and Munc13-4, we confirmed the interaction was direct and GTP-dependent *in vitro*.[4] Munc13-4 is a non-neuronal homolog of Munc13-1, a presynaptic protein essential for neurotrasmitter release. This structural similarity implies a critical role of Munc13-4 in platelet granule secretion.

To date, several Rab27 effector molecules, including synaptotagmin-like protein (Slp)-1–5 and Slp lacking C2 domain (Slac2)-a–c, have been documented.[9] All of these effectors interact with the GTP-bound form of Rab27 through their N-terminal conserved region, which is referred to as the Slp homology domain (SHD).[9] In terms of the GTP-Rab27 binding domain, Munc13-4 lacking the SHD is a distinct type of Rab27 effector.

Conclusion

Investigation of the molecular mechanism in platelet activation has been performed exclusively pharmacologically. Establishment of the semi-intact granule secretion and aggregation assays enabled us to examine the mechanism with molecular biological and biochemical methods. To elucidate the molecular mechanism would be to identify molecules involved in the regulation and to connect them temporally and spatially. We are going to continue this research project for better understanding of thrombus formation and for identifying potential targets for antiplatelet drugs.

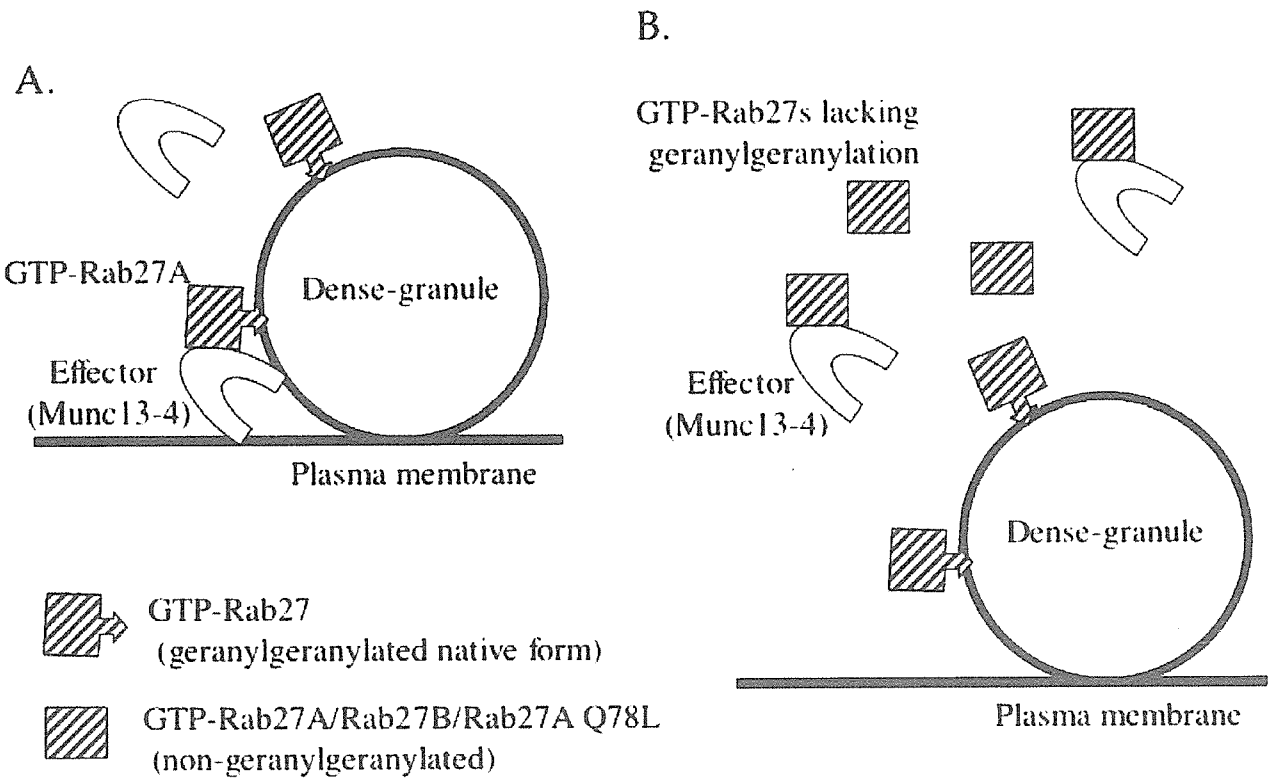

Figure 2 Functional model of GTP-Rab27/Munc13-4-mediated dense granule secretion in platelets. (A) GTP-bound active Rab27 interacts with its effector protein Munc13-4 to induce the granule secretion. (B) Addition of Rab27A, Rab27B or GTPase-deficient mutant Rab27AQ78L purified from *Escherichia coli*, which lacked post-translational modification with geranylgeranyl moiety and was unable to localize on the membrane of correct organelles, inhibited the secretion by sequestering its effector protein such as Munc13-4.

Acknowledgments

I express great gratitude for the support of the Novartis Foundation for Gerontological Research.

References

1 Horiuchi H. Recent advance in antiplatelet therapy: mechanisms, evidence and approach to the problems. *Ann Med* 2006; **38**: 162–172.
2 Tabuchi A, Yoshioka A, Higashi T *et al.* Identification of protein kinase Cα as an essential cytosolic factor for Ca2+-induced platelet aggregation. *J Biol Chem* 2003; **278**: 26 374–26 379.
3 Higashi T, Yoshioka A, Shirakawa R *et al.* Direct demonstration of involvement of the adaptor protein ShcA in the regulation of Ca^{2+}-induced platelet aggregation. *Biochem Biophys Res Commun* 2004; **322**: 700–704.
4 Shirakawa R, Higashi T, Tabuchi A *et al.* Munc13-4 is a GTP-Rab27 binding protein regulating dense core granule secretion in platelets. *J Biol Chem* 2004; **279**: 10 730–10 737.
5 Feldmann J, Callebaut I, Raposo G *et al.* Munc13-4 is essential for cytolytic granules fusion and is mutated in a form of familial hemophagocytic lymphohistiocytosis (FHL3). *Cell* 2003; **115**: 461–473.
6 Ishii E, Ueda I, Shirakawa R *et al.* Genetic subtypes of familial hemophagocytic lymphohistiocytosis: correlations with clinical features and cytotoxic T lymphocyte/natural killer cell functions. *Blood* 2005; **105**: 3442–3448.
7 Shirakawa R, Higashi T, Kondo H, Yoshiokal A, Kita T, Horiuchi H. Purification and functional analysis of a Rab27 effector Munc13-4 using a semi-intact platelet dense-granule secretion assay. *Methods Enzymol* 2005; **403**: 778–788.
8 Zerial M, McBride H. Rab proteins as membrane organizers. *Nat Rev Mol Cell Biol* 2001; **2**: 107–117.
9 Fukuda M. Versatile role of Rab27 in membrane trafficking: focus on the Rab27 effector families. *J Biochem (Tokyo)* 2005; **137**: 9–16.

Available online at www.sciencedirect.com
SCIENCE DIRECT
ELSEVIER
Biochemical and Biophysical Research Communications 344 (2006) 651–657
BBRC
www.elsevier.com/locate/ybbrc

Rab27a regulates epithelial sodium channel (ENaC) activity through synaptotagmin-like protein (SLP-5) and Munc13-4 effector mechanism

Sunil K. Saxena [a,*], Hisanori Horiuchi [b], Mitsunori Fukuda [c,d]

[a] *Center for Cell and Molecular Biology, Department of Chemistry and Chemical Biology, Stevens Institute of Technology, Hoboken, NJ 07030, USA*
[b] *Kyoto University, Kyoto, Japan*
[c] *Fukuda Research Initiative Unit, RIKEN, Wako, Japan*
[d] *Laboratory of Membrane Trafficking Mechanisms, Department of Developmental Biology and Neurosciences, Tohoku University, Aobayama, Aoba-ku, Sendai, Miyagi 980-8578, Japan*

Received 25 March 2006
Available online 7 April 2006

Abstract

Liddle's syndrome (excessive absorption of sodium ions) and PHA-1 (pseudohypoaldosteronism type 1) with decreased sodium absorption are caused by the mutations in the amiloride-sensitive epithelial sodium channel ENaC. Rab proteins are small GTPases involved in vesicle transport, docking, and fusion. Earlier, we reported that Rab27a inhibits ENaC-mediated currents through protein–protein interaction in HT-29 cells. We hereby report that Rab27a-dependent inhibition is associated with the GTP/GDP status as constitutively active or GTPase-deficient mutant Q78L inhibits amiloride-sensitive currents whereas GDP-locked inactive mutant T23N showed no effect. In order to further explore the molecular mechanism of this regulation, we performed competitive assays with two Rab27a-binding proteins: synaptotagmin-like protein (SLP-5) and Munc13-4 (a putative priming factor for exocytosis). Both proteins eliminate negative modulation of Rab27a on ENaC function. The SLP-5 reversal of Rab27a effect was restricted to C-terminal C2A/C2B domains assigned for putative phospholipids-binding function while the Rab27a-binding SHD motif imparted higher inhibition. The ENaC-mediated currents remain unaffected by Rab27a though SLP-5 appears to strongly bind it. The immunoprecipitation experiments suggest that in the presence of excessive Munc13-4 and SLP-5 proteins, Rab27a interaction with ENaC is diminished. Munc13-4 and SLP-5 limit the Rab27a availability to ENaC, thus minimizing its effect on channel function. These observations decisively prove that Rab27a inhibits ENaC function through a complex mechanism that involves GTP/GDP status, and protein–protein interactions involving Munc13-4 and SLP-5 effector proteins.

Keywords: ENaC; Rab27a; Trafficking; Munc13-4; SLP-5; GTP/GDP

Amiloride-sensitive channel (ENaC) is located in the apical membrane in tight epithelia and is associated with electrogenic sodium reabsorption. This channel performs a rate-limiting step in sodium reabsorption and control of its activity is crucial for the homeostasis of Na^+ balance and the maintenance of blood pressure [1,2]. Several ENaC regulatory mechanisms are known to exist, one of which is the recruitment of channel proteins to the cell surface from intracellular storage sites, while the other is protein–protein interaction [3–5].

Rab GTPases are critical elements of regulated endocytosis, exocytosis, and secretions [6,7]. The ability of Rab proteins to switch between the GTP- and GDP-bound conformations to inhabit active or inactive status [8,9] has a profound effect on their ability to perform highly defined, crucial, and specific responsibilities in the transport process [10–12]. Rab27a is expressed in a variety of specialized secretory cells, most of which undergo regulated exocytosis [13] viz. histamine release from rat basophilic leukemia 2H3 cells [14], melanosome [15,16], amylase [17], and regulated secretions in cytotoxic T lymphocytes [18]. The significance of Rab27a can be understood by the fact that the natural mutations of the Rab27a gene in human Griscelli syndrome

* Corresponding author. Fax: +1 201 216 8240.
E-mail address: ssaxena@stevens.edu (S.K. Saxena).

0006-291X/$ - see front matter © 2006 Elsevier Inc. All rights reserved.
doi:10.1016/j.bbrc.2006.03.160

[19–21] and in ashen mice have been reported to cause partial albinism and immunodeficiency which reflect the dysfunction of lysosome-related organelles [22]. Rab27a potentially constitutes a novel pharmacological target for the glucose competency in patients with diabetes mellitus [23].

Rab27a has been implicated in the regulation of different types of membrane trafficking. The Rab27a function depends largely on its GTP/GDP status and several newly identified binding partners, which perform effector functions in different cell types. These Rab27a-binding proteins are (1) the synaptotagmin-like proteins (SLP) family with tandem C2 Ca^{2+}-binding motifs, (2) SLaC2 family without any C2 motifs, and (3) Munc13-4, a putative priming factor for exocytosis. All SLP members basically share an N-terminal Rab27a-binding SLP-homology domain (SHD) and C-terminal tandem C2 domains (C2A and C2B), the putative phospholipids-binding domains. Munc13-4, on the other hand contains C2 motifs flanking inner C domains.

Initially, we reported that Rab27a inhibits ENaC activity in HT-29 cells [24,25] by protein–protein interaction and by impairing the channel expression at the plasma membrane. In this communication, we have characterized the molecular events by which Rab27a regulates sodium channel activity in HT-29 cells. In concurrence with our initial studies, we are providing the indomitable evidence to suggest that the regulatory mechanism involves effector proteins Munc13-4 and synaptotagmin-like proteins (SLP-5), both of which diminish ENaC-Rab27a interaction. Both effectors revert the Rab27a-dependent inhibition by reestablishing ENaC plasma membrane expression.

Materials and methods

Materials and reagents. Colonic epithelial HT-29 cells (HTB-38) were purchased from American type culture collection (ATCC, Manassas, VA). The α and γENaC antibodies have been described [25]. Lipofectamine was purchased from Invitrogen Life Technologies (Carlsbad, CA). GST antibody was purchased from GE (formerly Amersham Biosciences, Piscataway, NJ). Horseradish peroxidase-conjugated (HRP-conjugated) secondary antibodies (anti-rabbit and anti-mouse) were from Pierce Chemical Co. (Rockford, IL). Chariot® protein delivery system was available from Active Motif, (Carlsbad, CA). Rab27a antibody and the control and Rab27a-specific SiRNA were purchased from Santa Cruz Biotechnology, (Santa Cruz, CA).

Cell line. HT-29 cells were cultured in McCoy's 5a medium with 1.5 mM L-glutamine and 10% fetal bovine serum in 5% CO_2 at 37 °C. The cells were grown on Falcon 12 or 24 well inserts for all the experiments and maintained to determine the amiloride-sensitive ENaC-mediated currents. The cells were transfected with Rab, SLP, or Munc13-4 constructs using Lipofectamine (Gibco-BRL-Invitrogen) according to the manufacturer's instructions. The expression of each construct was confirmed by Western blot analysis for each set of reactions outlined in this communication.

Measurements of short circuit current (I_{sc}). ENaC-mediated currents were recorded two-ways. The I_{sc} were recorded with EVOM™ epithelial voltohmmeter using STX2 electrode (WPI, Sarasota, FL). Alternatively, the confluent monolayer was mounted in a modified Ussing chamber (Trans-24 miniperfusion chamber, Warner Instruments, Hamden, CT). Apical and basolateral chambers were continuously bathed with medium and I_{sc} were measured with transepithelial voltage clamped at 0 mV with a DVC-1000 dual voltage clamp. Voltage pulses (10 mV) were applied every 3 min to monitor the transepithelial resistance. After the initial measurements, 10 μM amiloride was added, and ENaC currents were expressed as the amiloride-sensitive component of the I_{sc}. To eliminate CFTR-dependent currents all measurements were made in the presence of 1 mM diphenyl carboxylate (DPC).

Biotinylation of cell-surface proteins. HT-29 cells were transfected with Rab27a cDNA constructs using Lipofectamine as per the manufacturer's instructions (Invitrogen). Two days after transfection, the cells were washed with PBS three times, and then incubated in 5 mL of cell impermeant Sulfo-NHS-SS-Biotin (Pierce Biotechnology Inc., Rockford, IL) (0.5 mg/mL) at 4 °C for 30 min. After 30 min of incubation, the reaction was stopped by quenching with Tris-buffered saline (TBS), the cells were solubilized in RIPA buffer, and the lysate was centrifuged at 14,000 rpm for 5 min at 4 °C to collect the supernatant and its protein concentration was determined. Then, equal amounts of the lysate from each sample were mixed with 200 μL of streptavidin–agarose beads (5% slurry in PBS). The samples were incubated overnight at 4 °C with gentle rocking, and centrifuged at 8000*g* for 2 min to collect the supernatant. The beads carrying biotinylated proteins were washed with RIPA buffer five times. Finally, the biotinylated proteins were eluted from the beads by the addition of SDS-sample buffer. Equal volumes of the eluted proteins in sample buffer were loaded on a gel. The samples were analyzed for ENaC expression by Western blot analysis using an α or γENaC antibody. The blots were raised using Enhanced Chemiluminescence (ECL) and the films were developed using autoradiography.

Immunoprecipitation experiments. Cell lysates in RIPA buffer (1% NP-40 or Triton X-100, 1% sodium deoxycholate, 1 mM EDTA, 0.1% SDS, 0.15 mol NaCl, 0.01 M sodium phosphate (pH 7.2), 1% trasylol, a 1:100 dilution with 100 mg/mL leupeptin, and 100 mM phenylmethylsulfonyl fluoride) were centrifuged to recover the supernatant at 14,000-rpm for 5 min. The lysates were precleared by incubating with protein A–Sepharose beads for 1 h at 4 °C. The supernatants were further incubated with a specific antibody for 2 h at 4 °C and followed by incubation with Sepharose beads (Sigma, St. Louis, MO) for 2 h at 4 °C. After washing with RIPA buffer and centrifugation at 10,000*g* for 15 s, beads were solubilized in SDS-sample buffer and run on SDS–PAGE. The proteins were transferred to a PVDF membrane. The bound antibody was detected by ECL and quantitated by phosphor-imaging under conditions where there was a linear relationship between intensity and pixel number. In some cases, membranes were stripped of bound antibodies and re-probed with additional antibodies. Following the manufacturer's instructions, membranes were immersed in stripping buffer (62.5 mM Tris–HCl (pH 6.7), 2% SDS, and 100 mM β-mercaptoethanol) for 30 min at 55 °C, and washed extensively in Tris-buffered saline (0.1 M, pH 7.4; 0.05% Tween 20) at room temperature. Membranes were re-blocked in milk-TBS and incubated with the desired antibody and raised for protein detection using ECL as described above.

SiRNA studies. The control and Rab27a-specific SiRNA were used in the study. The control SiRNA contained the sequence that does not interfere in the expression of any known mRNA. The SiRNA effect was confirmed by Western blot analysis of transfected cells. One hundred nanomolars SiRNA (final conc.) was mixed with 20 μL of the transfection medium reagent per well and incubated at room temperature. In another vial, 1.2 μL of the transfection reagent was mixed with 20 μL transfection medium and incubated. The contents of both vials were mixed and incubated. After 20 min, the contents were mixed with 160 μL of the transfection medium and this solution was laid on top of the cells in each well. The cells growing on inserts in a 24-well plate (~50% confluent for this experiment) were used for this experiment. The plate was incubated in 37 °C with 5% CO_2 for 5–7 h, and then 200 μL of the culture medium with double serum was added on top of the inserts. The ENaC-mediated amiloride-sensitive currents were recorded 24 h post-SiRNA transfection as described before.

Purification of SLP proteins. PGEX-SLP-C2A, C2B, and SHD proteins were isolated for bacterial cultures expressing the respective cDNA. The proteins were purified using glutathione beads (Amersham-Glutathione Sepharose™ 4B). The beads were washed with phosphate-buffered saline (0.15 M, pH 7.3), and then a 50% slurry of beads was incubated with bacterial lysates (isolated by cell lysis) at 4 °C overnight. Following

incubation, the beads were washed twice with PBS and once with RIPA buffer. The SLP proteins were eluted from the beads by adding 100 μL elution buffer (50 mM Tris, 10 mM glutathione, pH 8.0) to the beads, incubating 10–15 min at room temperature and then centrifuged at 5000 rpm for 5 min to collect the supernatant. The protein concentration was determined by bicinchoninic acid (BCA) assay.

Introduction of proteins using Chariot® delivery system. SLP proteins were mixed in a complex with the Chariot® reagent (diluted in 70% DMSO) at a ratio of 20 μg protein: 10 μL in 100 μL PBS for 30 min at RT. The protein:Chariot®complexes were overlaid onto cultured cells in the presence of fresh serum free medium and incubated at 37 °C for 1 h followed by incubation for 2 more hours in the presence of complete growth medium.

Statistical analysis. A paired test or analysis of variance for multiple comparisons was used for the statistical analysis. A p value of less than 0.05 was considered significant.

Results

This communication describes the basic mechanism by which Rab27a inhibits amiloride-sensitive ENaC. The study also addresses the role of GDP-locked (inactive) and GTP-active Rab27a mutants. Additionally, this study defines the molecular machinery involved in Rab27a regulation of ENaC. The study signifies that Rab27a-binding partners, Munc13-4, and synaptotagmin-like proteins (SLP-5), reverse the negative regulation of ENaC by Rab27a by diminishing channel interaction with Rab27a, by ultimately enhancing plasma membrane channel expression.

Rab27a inhibits channel function by a GTP/GDP dependent mechanism

The over-expression of the inactive (GDP-locked) form of Rab27a (T23N) showed no inhibition of amiloride-sensitive currents recorded otherwise with the wild-type Rab27a. However, the constitutively, active isoform of Rab27a, Q78L (GTP-locked) showed the inhibition (Fig. 1). The smaller inhibition with this isoform possibly suggests that the effect of Rab27a-dependent inhibition is quite complex and revolves around the GTP/GDP exchanges or its active or inactive status. It needs to be stated that Rab27a is expressed in HT-29 cells and therefore the over-expressed Rab protein is competing with native Rab27a for the available GTP/GDP pool in the cell under a defined condition. The GTP status of each was confirmed by GTP overlay assay (data not shown).

Munc13-4 reverses Rab27a inhibition of amiloride-sensitive currents

Several recent studies have provided the evidence to suggest that Munc13-4 is a highly specific-binding partner of Rab27a. In order to specify the role of this protein in the Rab27a-dependent effect on ENaC function, we co-transfected HT-29 cells expressing Rab27a with Munc13-4 and recorded the amiloride-sensitive currents. As indicated in Fig. 2, we recorded the net reversal of inhibition of amiloride-sensitive currents observed otherwise with Rab27a alone. The immunoprecipitation studies further suggested that Rab27a weakly binds to ENaC in the presence of Munc13-4 suggesting that Rab27a inhibits ENaC activity in HT-29 cells by protein–protein interactions.

Synaptotagmin-like proteins partially reverse ENaC inhibition by Rab27a

Synaptotagmin-like proteins (SLP) have been characterized as specific-binding partners of Rab27a. These proteins are characterized by the presence of C2A-, C2B-binding motifs, and SHD domains. Upon transfection, the reversal of amiloride-sensitive currents was noticed with constructs carrying only C2A and C2B domains, while SHD motif expression exhibited little more inhibition (Fig. 3). The reversal of currents by C2A or C2B motifs, which are involved in binding with phospholipids suggest the

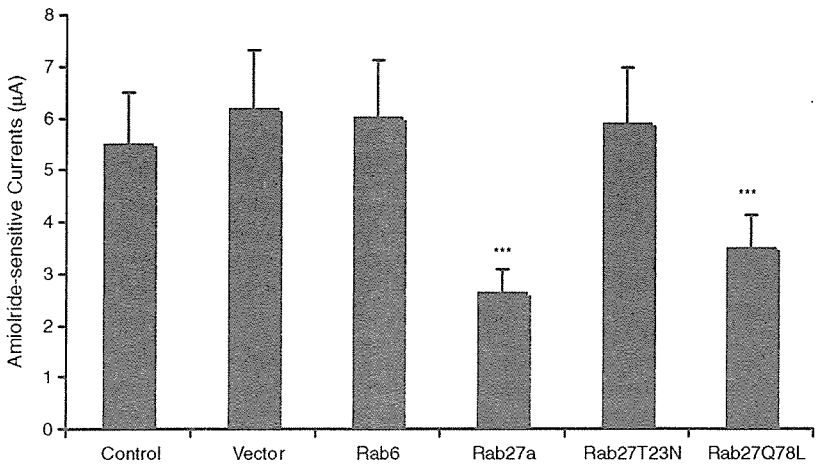

Fig. 1. The monolayer of HT-29 cells grown on cell inserts were transiently transfected with Rab cDNA using Lipofectamine and the amiloride-sensitive currents were recorded two days later as described in the text. Data are means of three individual experiments. Asterisks represent the statistical significance with a p value <0.05.

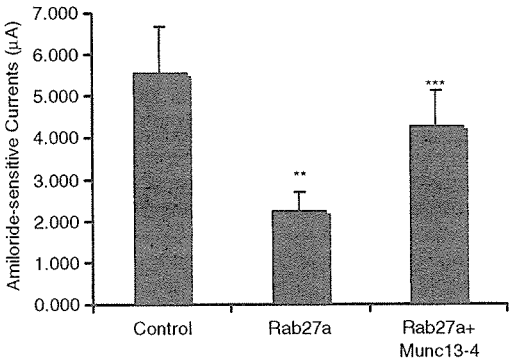

Fig. 2. Munc13-4 reverses Rab27a inhibition of amiloride-sensitive currents. HT-29 cells were transfected with wild-type Rab27a and Munc13-4 cDNA and the amiloride-sensitive currents were recorded 48 h later. The data are means of three individual experiments performed. A significant change ($p < 0.05$) from the control is denoted by two asterisks while the values denoted by three asterisks in Munc13-4 co-injected cells define the significance against Rab27a (middle bar) inhibited values.

necessity of the membrane for the attachment of the complex in addition to the requirement of SHD for Rab27a binding. The higher inhibition recorded with SHD domains further illustrates the significance of membrane attachment. These Rab27a-binding proteins (i.e., the synaptotagmin-like protein (SLP) family with tandem C2 Ca^{2+}-binding motifs, and Munc13-4, a putative priming factor for exocytosis) provide a crucial understanding of the molecular mechanism by which Rab27a regulates the membrane trafficking of ENaC.

SLP and Munc13-4 impair ENaC ability to interact with Rab27a

In order to assess the mechanism by which synaptotagmin-like proteins (SLP-5) and Munc13-4 reverse the

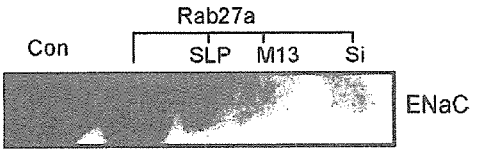

Fig. 4. SLP-5 and Munc13-4 reduce ENaC interaction with Rab27a. SLP-5 and Munc13-4 proteins were expressed in HT-29 cells transfected with Rab27a by transfection and Chariot® delivery system, respectively. Cell lysates in RIPA buffer were centrifuged to recover the supernatant and the lysates were incubated with protein A–Sepharose beads and Rab27a antibody for 2 h at 4 °C. The beads were solubilized in SDS-sample buffer and run on SDS–PAGE, transferred to a PVDF membrane. The blots were probed with αENaC antibody and raised with ECL and the films were developed using autoradiography.

regulated expression of ENaC at the cell surface, we employed two techniques to address this issue. At first we transfected cells with Rab27a and one of these proteins and then immunoprecipitated the proteins with Rab27a antibody, and then probed the immunoblots with αENaC antibody. Our data suggest that in the presence of SLP-5 and Munc13-4, the ENaC density is diminished in a long way from the control suggesting that both these proteins abolish the interaction between ENaC and Rab27a (Fig. 4). Concomitantly, we observed intense interaction of Rab27a with SLP and Munc13-4. Second, we show that these proteins revert the Rab27a effect by promoting the ENaC exocytosis to the plasma membrane.

SLP and Munc13-4 reestablish ENaC expression at the cell surface

Our previous observations suggested that the intense binding efficiency of SLP and Munc13-4 with Rab27a might promote the expression of ENaC at the cell surface due to the limited availability of Rab27a to interact with ENaC. Second, in continuation with our previous finding

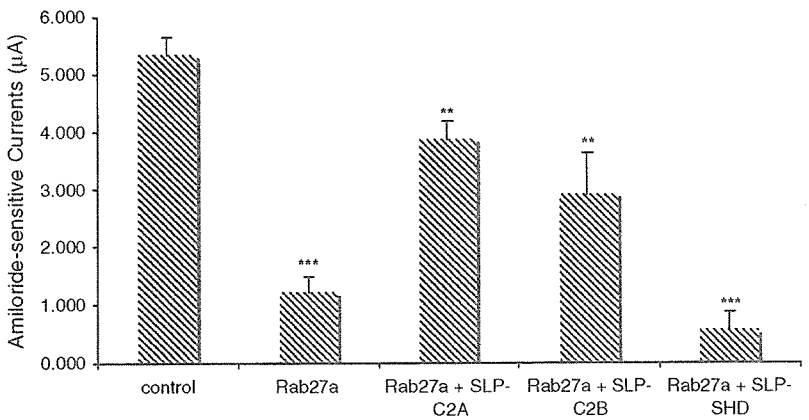

Fig. 3. Rab27a-dependent inhibition is reversed by synaptotagmin-like protein (SLP). The purified SLP proteins were introduced into HT-29 monolayers using Chariot® delivery system. SLP-GST proteins, purified using glutathione followed by dialysis, were mixed in a complex with the Chariot® reagent at a ratio of 20 μg protein: 10 μL in 100 μL PBS and the protein:Chariot® complexes were overlaid onto cultured cells in serum free medium and incubated at 37 °C for 1 h followed by 2 more hours in presence of complete growth medium. The ENaC-mediated currents were recorded 48 h later. Data are means of six individual wells under each condition. A significant change ($p < 0.05$) from the control values is denoted by three asterisks while values with two asterisks denote a significant change from Rab27a (second bar) inhibited currents.

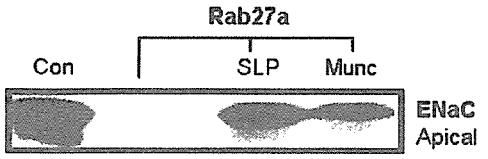

Fig. 5. SLP-5 and Munc13-4 increase plasma membrane ENaC expression in the presence of Rab27a. SLP-5 and Munc13-4 proteins were expressed in HT-29 cells transfected with Rab27a by transfection and Chariot® delivery system, respectively. Two days later, the cells were washed with PBS, and then incubated with cell impermeant Sulfo-NHS-SS-Biotin (0.5 mg/mL) at 4 °C for 30 min. After 30 min of incubation, the reaction was stopped by quenching, and the cells were solubilized in RIPA buffer. The lysates were centrifuged to collect the supernatant. Equal amounts of the lysate from each sample were mixed with 200 μL of streptavidin–agarose beads and incubated overnight at 4 °C. The beads carrying biotinylated proteins were washed with RIPA buffer, eluted by the addition of SDS-sample buffer, and analyzed by SDS–PAGE. The samples were analyzed by Western blot analysis using the αENaC antibody. The blots were raised using enhanced chemiluminescence (ECL) and the films were developed using autoradiography.

that the reduction in ENaC-mediated currents in the cells over-expressed with Rab27a protein was due to reduced ENaC at the cell surface, we biotinylated the cell-surface proteins by employing cell impermeant Sulfo-NHS-SS-Biotin and pulled down the complex with streptavidin–agarose. In line with our hypothesis, we observed reduction in the abundance of ENaC in the cells expressing Rab 27a (Fig. 5). However, in the presence of SLP and Munc13-4, the ENaC expression is increased at the cell surface. These data further support that Rab27a modulates ENaC transport to the cell surface by either retaining the channel proteins intracellular or incapacitating its expression at the cell surface. SLP-5 and Munc13-4 due to their stronger affinity for Rab27a incapacitate the ENaC-Rab27a interaction and therefore channel density at the plasma membrane is increased resulting in the reversal of amiloride-sensitive currents or ENaC inhibition.

Discussion

We had earlier described the ENaC regulation by Rab27a, and provided several lines of evidence to suggest that it is due to the physical interaction of channel proteins with Rab27a, with the impairment of ENaC expression at the plasma membrane resulting in reduced channel expression at apical membrane with the concommittant increase in the cytosolic ENaC pool. This communication explores the molecular mechanism associated with ENaC/Rab27a interaction. Our data suggest that (i) Rab27a inhibits ENaC activity due to its association with the channel proteins through protein–protein interactions, which is reflected in the decreased expression of the channel at the cell surface, since Rab27a is primarily involved in lysosomal trafficking. (ii) Rab27a inhibition of channel activity could be abolished in the presence of two active components that are Rab27a-binding partners Munc13-4 and synaptotagmin-like proteins (SLP-5). These proteins, when over-expressed, interact tightly with Rab27a and abort the availability of Rab27a for ENaC interaction, and finally (iii) both effectors reestablish ENaC presence at the plasma membrane in spite of over-expressed Rab27a.

Folding, maturation, and trafficking of transmembrane proteins from the ER to their ultimate destination, the plasma membrane is a regulated translocation of transport vesicles [26,27]. Subsequently, vesicular fusion with the target membrane results in increased channel density due to the ability of multiple Rabs to control the regularized traffic at the cell surface [6,28]. The trafficking and the assembly of the ENaC channel is critical in understanding its regulation. Under normalized physiologic conditions native ENaC recycles from early endosomes back to the cell surface [29], while the proteosomal degradation characterizes its degradation route. The association of Rab27a with ENaC translocation coupled with the lysosomal compartmentalization of this Rab isoform suggests an alternate route for ENaC degradation.

In addition to its localization on secretory granules, Rab27a is also predominantly expressed on lysosomes [30–33]. Due to the varied nature of regulation being effected by Rab27a which has been implicated in the regulation of different types of membrane trafficking, the most obvious question is how does the Rab27a protein regulate these different types of membrane trafficking? Rab27a has several binding partners or effector proteins.

It has earlier been established that SLP-5 is a novel Rab27a effector [34,35]. The isoform SLP-5 exceptionally binds several Rabs including Rab3 and Rab27a in vitro, but it preferentially interacts with Rab27 isoforms in living cells [36,37]. Another Rab effector, Rabphilin previously characterized as the Rab3 effector, is also believed to function as a Rab27a effector [22,38]. Results have indicated that the SHD motifs of SLP function as a Rab27a-binding domain [39]. Several pieces of evidence also point to the involvement of the Rab27a and its effector complex with the proteins that are essential for membrane transport and fusion, such as syntaxin1A and Munc18-1, though we could not detect the presence of these proteins in the Rab27a pull-down complex [40]. Not surprisingly, the SLP proteins possess the conserved N-terminal Rab27a-binding domain and show Rab27a-binding activity in vitro or when over-expressed in cell lines [41]. SLP appear to interact with both Rab27a(T23N), a dominant negative form that mimics the GDP-bound form, and Rab27a(Q78L), a dominant active form that mimics the GTP-bound form.

Unlike other members, Munc13-4 lacks an N-membrane-binding domain. Munc13-4 is hypothesized to contain a novel Rab27a-binding domain. Rab27a-binding protein Munc13-4 has been purified from the platelet cytosolic fraction with GTP-Rab27a-immobilized beads [42]. Munc13-4 is a direct partner of Rab27a, as it does not bind to other GTPases [42]. The two proteins are highly expressed in several tissues and cell lines where they colocalize on secretory lysosomes. More so, the Munc13-4

homology domains are essential for the localization of Munc13-4 in the secretory lysosomes [43]. We believe that the Rab27a/Munc13-4 interaction is an essential regulator of channel proteins with the plasma membrane in epithelial cells as observed in mast cells, platelets, and histamine release [14]. However, it appears that the Munc13-4 effect is independent of membrane involvement.

In conclusion, Rab27a physical interaction with ENaC defines its effect on channel function. The negative regulation of ENaC function is the consequence of depleted appearance of channel at the plasma membrane. Given the Rab27a association with exocytosis and lysosomal trafficking [41,44,45], it is conceivable that Rab isoforms are involved in inter-compartmental translocation and the assembly of ENaC. The ability of Munc13-4 (a priming exocytosis factor) and SLP-5, to reverse the inhibitory effect of Rab27a is due to the ability of these over-expressed proteins to preferentially associate with Rab27a, and depriving its ability to bind ENaC. We confirmed this possibility by utilizing immunoprecipitation studies as a part of protein–protein interaction. The increased surface expression of ENaC in Munc13-4 or SLP cotransfected cells corroborate our previous contention that Rab27a is a major trafficking protein associated with ENaC expression at the plasma membrane. Moreover, the results with the C2 domains of SLP in conjunction with the GTP/GDP current recordings open a possibility that the vesicles with channel proteins are docked at the plasma membrane as a readily releasable pool as proposed recently for dense core vesicle exocytosis [40]. We have further characterized the colocalization of ENaC and Rab27a predominantly in three compartments in the following order; plasma membrane<microsome<lysosome (data not shown), suggesting that Rab27a diverts the ENaC complex away from the plasma membrane. Although our studies did not address a vital issue related to ENaC mutants of Liddle's syndrome or PHA-1, which display impaired trafficking, these studies are vital to explore the possibility of Rab involvement in the regulated exocytosis of diseased forms. It is likely that some sort of protein–protein interaction may provide a therapeutic approach to regulating ENaC activity associated with Liddle's syndrome.

The Rab27a/effector system is reportedly involved in the glucose-specific signals for the exocytosis of insulin granules in pancreatic beta cells [30]. It appears that Rab27 regulates various exocytotic pathways in addition to its recently identified role in lysosome-related trafficking using multiple organelle-specific effector proteins like SLaC2, SLP, or Munc13-4 [41]. Given the relative expression of Rab27a in specialized cell types in the pathogenesis of Griscelli syndrome [32], where the Rab27a/Munc13-4 complex is an essential regulator of secretory granule fusion with the plasma membrane in cytotoxic T lymphocytes [43], it is likely that Rab27a exhibits essentially similar credentials in epithelial cell systems controlling the exocytosis of ion channels.

Acknowledgments

Authors are thankful to Constantine George, Simarna Kaur, and Madhurima Singh for technical support throughout the study. The authors also acknowledge the technical assistance by Amanda Rogers. This work is supported in part by the Grant (DK57717) funded to SKS by National Institute of Digestive & Diabetes & Kidney Disease (NIDDK), Bethesda, MD.

References

[1] P.M. Snyder, Minireview: regulation of epithelial Na+ channel trafficking, Endocrinology 146 (2005) 5079–5085.
[2] E. Hummler, Epithelial sodium channel, salt intake, and hypertension, Curr. Hypertens. Rep. 5 (2003) 11–18.
[3] K. Gormley, Y. Dong, G.A. Sagnella, Regulation of the epithelial sodium channel by accessory proteins, Biochem. J. 371 (2003) 1–14.
[4] P.M. Snyder, The epithelial Na+ channel: cell surface insertion and retrieval in Na+ homeostasis and hypertension, Endocr. Rev. 23 (2002) 258–275.
[5] D. Rotin, Regulation of the epithelial sodium channel (ENaC) by accessory proteins, Curr. Opin. Nephrol. Hypertens. 9 (2000) 529–534.
[6] E.S. Ward, C. Martinez, C. Vaccaro, J. Zhou, Q. Tang, R.J. Ober, From sorting endosomes to exocytosis: association of Rab4 and Rab11 GTPases with the Fc receptor, FcRn, during recycling, Mol. Biol. Cell (2005).
[7] A. Spang, Vesicle transport: a close collaboration of Rabs and effectors, Curr. Biol. 14 (2004) R33–R34.
[8] E. Korobko, S. Kiselev, S. Olsnes, H. Stenmark, I. Korobko, The Rab5 effector Rabaptin-5 and its isoform Rabaptin-5delta differ in their ability to interact with the small GTPase Rab4, FEBS J. 272 (2005) 37–46.
[9] G. Zhu, P. Zhai, J. Liu, S. Terzyan, G. Li, X.C. Zhang, Structural basis of Rab5-Rabaptin5 interaction in endocytosis, Nat. Struct. Mol. Biol. 11 (2004) 975–983.
[10] B. Short, F.A. Barr, Membrane fusion: caught in a trap, Curr. Biol. 14 (2004) R187–R189.
[11] H. Stenmark, V.M. Olkkonen, The Rab GTPase family, Genome Biol. 2 (2001) 3007, REVIEWS.
[12] A.J. Molendijk, B. Ruperti, K. Palme, Small GTPases in vesicle trafficking, Curr. Opin. Plant Biol. 7 (2004) 694–700.
[13] T. Tolmachova, R. Anders, J. Stinchcombe, G. Bossi, G.M. Griffiths, C. Huxley, M.C. Seabra, A general role for Rab27a in secretory cells, Mol. Biol. Cell 15 (2004) 332–344.
[14] K. Goishi, K. Mizuno, H. Nakanishi, T. Sasaki, Involvement of Rab27 in antigen-induced histamine release from rat basophilic leukemia 2H3 cells, Biochem. Biophys. Res. Commun. 324 (2004) 294–301.
[15] C.E. Futter, J.S. Ramalho, G.B. Jaissle, M.W. Seeliger, M.C. Seabra, The role of Rab27a in the regulation of melanosome distribution within retinal pigment epithelial cells, Mol. Biol. Cell 15 (2004) 2264–2275.
[16] Y. Chen, P. Samaraweera, T.T. Sun, G. Kreibich, S.J. Orlow, Rab27b association with melanosomes: dominant negative mutants disrupt melanosomal movement, J. Invest. Dermatol. 118 (2002) 933–940.
[17] A. Imai, S. Yoshie, T. Nashida, H. Shimomura, M. Fukuda, The small GTPase Rab27B regulates amylase release from rat parotid acinar cells, J. Cell Sci. 117 (2004) 1945–1953.
[18] J.C. Stinchcombe, D.C. Barral, E.H. Mules, S. Booth, A.N. Hume, L.M. Machesky, M.C. Seabra, G.M. Griffiths, Rab27a is required for regulated secretion in cytotoxic T lymphocytes, J. Cell Biol. 152 (2001) 825–834.
[19] W. Westbroek, J. Lambert, S. De Schepper, R. Kleta, K. Van Den Bossche, M.C. Seabra, M. Huizing, M. Mommaas, J.M. Naeyaert,

Rab27b is up-regulated in human Griscelli syndrome type II melanocytes and linked to the actin cytoskeleton via exon F-Myosin Va transcripts, Pigment Cell Res. 17 (2004) 498–505.
[20] F. Schuster, D.K. Stachel, I. Schmid, F.A. Baumeister, U.B. Graubner, M. Weiss, R.J. Haas, B.H. Belohradsky, Griscelli syndrome: report of the first peripheral blood stem cell transplant and the role of mutations in the RAB27A gene as an indication for BMT, Bone Marrow Transplant. 28 (2001) 409–412.
[21] G. Menasche, E. Pastural, J. Feldmann, S. Certain, F. Ersoy, S. Dupuis, N. Wulffraat, D. Bianchi, A. Fischer, F. Le Deist, G. de Saint Basile, Mutations in RAB27A cause Griscelli syndrome associated with haemophagocytic syndrome, Nat. Genet. 25 (2000) 173–176.
[22] M. Fukuda, Versatile role of Rab27 in membrane trafficking: focus on the Rab27 effector families, J. Biochem. (Tokyo) 137 (2005) 9–16.
[23] T. Aizawa, M. Komatsu, Rab27a: a new face in beta cell metabolism-secretion coupling, J. Clin. Invest. 115 (2005) 227–230.
[24] S. Saxena, M. Singh, K. Engisch, M. Fukuda, S. Kaur, Rab proteins regulate epithelial sodium channel activity in colonic epithelial HT-29 cells, Biochem. Biophys. Res. Commun. 337 (2005) 1219–1223.
[25] S.K. Saxena, M. Singh, H. Shibata, S. Kaur, C. George, Rab4 GTP/GDP modulates amiloride-sensitive sodium channel (ENaC) function in colonic epithelia, Biochem. Biophys. Res. Commun. 340 (2006) 726–733.
[26] N. Ballatori, C.L. Hammond, J.B. Cunningham, S.M. Krance, R. Marchan, Molecular mechanisms of reduced glutathione transport: role of the MRP/CFTR/ABCC and OATP/SLC21A families of membrane proteins, Toxicol. Appl. Pharmacol. 204 (2005) 238–255.
[27] S.W. Kim, W. Wang, J. Nielsen, J. Praetorius, T.H. Kwon, M.A. Knepper, J. Frokiaer, S. Nielsen, Increased expression and apical targeting of renal ENaC subunits in puromycin aminonucleoside-induced nephrotic syndrome in rats, Am. J. Physiol. Renal. Physiol. 286 (2004) F922–F935.
[28] Y. Zhang, A. Foudi, J.F. Geay, M. Berthebaud, D. Buet, P. Jarrier, A. Jalil, W. Vainchenker, F. Louache, Intracellular localization and constitutive endocytosis of CXCR4 in human CD34+ hematopoietic progenitor cells, Stem Cells 22 (2004) 1015–1029.
[29] O. Staub, I. Gautschi, T. Ishikawa, K. Breitschopf, A. Ciechanover, L. Schild, D. Rotin, Regulation of stability and function of the epithelial Na+ channel (ENaC) by ubiquitination, EMBO J. 16 (1997) 6325–6336.
[30] K. Kasai, M. Ohara-Imaizumi, N. Takahashi, S. Mizutani, S. Zhao, T. Kikuta, H. Kasai, S. Nagamatsu, H. Gomi, T. Izumi, Rab27a mediates the tight docking of insulin granules onto the plasma membrane during glucose stimulation, J. Clin. Invest. 115 (2005) 388–396.
[31] Z. Yi, H. Yokota, S. Torii, T. Aoki, M. Hosaka, S. Zhao, K. Takata, T. Takeuchi, T. Izumi, The Rab27a/granuphilin complex regulates the exocytosis of insulin-containing dense-core granules, Mol. Cell. Biol. 22 (2002) 1858–1867.
[32] D.C. Barral, J.S. Ramalho, R. Anders, A.N. Hume, H.J. Knapton, T. Tolmachova, L.M. Collinson, D. Goulding, K.S. Authi, M.C. Seabra, Functional redundancy of Rab27 proteins and the pathogenesis of Griscelli syndrome, J. Clin. Invest. 110 (2002) 247–257.
[33] M.J. Hannah, A.N. Hume, M. Arribas, R. Williams, L.J. Hewlett, M.C. Seabra, D.F. Cutler, Weibel-Palade bodies recruit Rab27 by a content-driven, maturation-dependent mechanism that is independent of cell type, J. Cell Sci. 116 (2003) 3939–3948.
[34] T.S. Kuroda, M. Fukuda, H. Ariga, K. Mikoshiba, Synaptotagmin-like protein 5: a novel Rab27A effector with C-terminal tandem C2 domains, Biochem. Biophys. Res. Commun. 293 (2002) 899–906.
[35] M. Fukuda, Distinct Rab27A binding affinities of Slp2-a and Slac2-a/melanophilin: Hierarchy of Rab27A effectors, Biochem. Biophys. Res. Commun. 343 (2006) 666–674.
[36] M. Fukuda, E. Kanno, C. Saegusa, Y. Ogata, T.S. Kuroda, Slp4-a/granuphilin-a regulates dense-core vesicle exocytosis in PC12 cells, J. Biol. Chem. 277 (2002) 39673–39678.
[37] T.S. Kuroda, M. Fukuda, Rab27A-binding protein Slp2-a is required for peripheral melanosome distribution and elongated cell shape in melanocytes, Nat. Cell Biol. 6 (2004) 1195–1203.
[38] M. Fukuda, E. Kanno, A. Yamamoto, Rabphilin and Noc2 are recruited to dense-core vesicles through specific interaction with Rab27A in PC12 cells, J. Biol. Chem. 279 (2004) 13065–13075.
[39] T.S. Kuroda, M. Fukuda, H. Ariga, K. Mikoshiba, The Slp homology domain of synaptotagmin-like proteins 1–4 and Slac2 functions as a novel Rab27A binding domain, J. Biol. Chem. 277 (2002) 9212–9218.
[40] T. Tsuboi, M. Fukuda, The Slp4-a linker domain controls exocytosis through interaction with Munc18-1. Syntaxin1a complex, Mol. Biol. Cell (2006) (In press). Available online 15 February 2006.
[41] T. Izumi, H. Gomi, K. Kasai, S. Mizutani, S. Torii, The roles of Rab27 and its effectors in the regulated secretory pathways, Cell. Struct. Funct. 28 (2003) 465–474.
[42] R. Shirakawa, T. Higashi, A. Tabuchi, A. Yoshioka, H. Nishioka, M. Fukuda, T. Kita, H. Horiuchi, Munc13-4 is a GTP-Rab27-binding protein regulating dense core granule secretion in platelets, J. Biol. Chem. 279 (2004) 10730–10737.
[43] M. Neeft, M. Wieffer, A.S. de Jong, G. Negroiu, C.H. Metz, A. van Loon, J. Griffith, J. Krijgsveld, N. Wulffraat, H. Koch, A.J. Heck, N. Brose, M. Kleijmeer, P. van der Sluijs, Munc13-4 is an effector of rab27a and controls secretion of lysosomes in hematopoietic cells, Mol. Biol. Cell 16 (2005) 731–741.
[44] G. Bossi, S. Booth, R. Clark, E.G. Davis, R. Liesner, K. Richards, M. Starcevic, J. Stinchcombe, C. Trambas, E.C. Dell'angelica, G.M. Griffiths, Normal lytic granule secretion by cytotoxic t lymphocytes deficient in BLOC-1, -2 and -3 and Myosins Va, VIIa and XV, Traffic 6 (2005) 243–251.
[45] M. Zerial, H. McBride, Rab proteins as membrane organizers, Nat. Rev. Mol. Cell Biol. 2 (2001) 107–117.

Asymmetric Coiled-Coil Structure with Guanine Nucleotide Exchange Activity

Yusuke Sato,[1] Ryutaro Shirakawa,[2] Hisanori Horiuchi,[2] Naoshi Dohmae,[3] Shuya Fukai,[1,4,*] and Osamu Nureki[1,*]
[1] Department of Biological Information, Graduate School of Bioscience and Biotechnology, Tokyo Institute of Technology, 4259 Nagatsuta-cho, Midori-ku, Yokohama-shi, Kanagawa 226-8501, Japan
[2] Department of Cardiovascular Medicine, Graduate School of Medicine, Kyoto University, 54 Kawara-machi, Shogoin, Sakyo-ku, Kyoto 606-8507, Japan
[3] Biomolecular Characterization, RIKEN, 2-1 Hirosawa, Wako-shi, Saitama 351-0198, Japan
[4] Center for Biological Resources and informatics, Tokyo Institute of Technology, 4259 Nagatsuta-cho, Midori-ku, Yokohama-shi, Kanagawa 226-8501, Japan
*Correspondence: sfukai@bio.titech.ac.jp (S.F.), nureki@bio.titech.ac.jp (O.N.)
DOI 10.1016/j.str.2007.01.003

SUMMARY

Vesicular traffic during exocytosis is regulated by Rab GTPase, Sec4p in yeast, which is activated by a guanine nucleotide exchange factor (GEF) called Sec2p. The GEF activity is localized in the N-terminal 160 residues of Sec2p, which lacks sequence similarity with any other GEFs with known structures, and thereby the guanine nucleotide exchange mechanism by Sec2p remains unknown. Here, we report the crystal structure of the Sec2p GEF domain at 3.0 Å resolution. The structure unexpectedly consists of a homodimeric, parallel coiled coil that extends over 180 Å. Pull-down and guanine nucleotide exchange analyses on a series of deletion and point mutants of Sec2p unveiled the catalytic residues for its GEF activity as well as the Sec4p binding site, thus presenting a nucleotide exchange mechanism by a simple coiled coil. The present functional analyses allow us to build the Sec2p:Sec4p complex model, which explains the specificity for Rab GTPases by their respective GEF proteins.

INTRODUCTION

In eukaryotic cells, various biological molecules are transported and secreted by secretory vesicles, which fuse with the plasma membrane in a process called exocytosis. The exocytotic events are regulated by interactions between Ras-related small GTPases, such as Rho, Rab, and Ral, and their respective effectors (Lipschutz and Mostov, 2002). These small GTPases shuttle between the active GTP-bound and inactive GDP-bound states, which differ mainly in the conformations of two loop regions, called "switch I" and "switch II." The downstream effectors of the small GTPases discriminate the conformational differences in the switch regions and specifically bind with the GTP-bound form. Therefore, this conformational transition is essential for the small GTPase functions (Takai et al., 2001).

In *Saccharomyces cerevisiae*, genes whose mutation causes dysfunctional secretion have been genetically identified as "*sec*." Sec4p, the equivalent of the mammalian Rab GTPase, regulates the transport of secretory vesicles (Guo et al., 1999). In a GTP-dependent fashion, Sec4p interacts with Sec15p, a component of the multiprotein complex, Exocyst, which reportedly tethers the secretory vesicle to a defined site of the plasma membrane: this Sec4p•Sec15p interaction is essential for the Exocyst assembly (TerBush et al., 1996). After membrane fusion, Sec4p hydrolyzes its bound GTP to GDP and is released into the cytoplasm, where it reassociates with a new secretory vesicle to get ready for the next round of membrane fusion. This Sec4p localization is controlled by two types of functional regulators: a GTPase-activating protein (GAP) accelerates the GTP hydrolysis activity of Sec4p, while a guanine nucleotide exchange factor (GEF) catalyzes the GDP release from Sec4p to convert it into the activated, GTP-bound form. Sec2p (759 amino acids, Mw 105 kDa) has been identified as the GEF for Sec4p in yeast (Walch-Solimena et al., 1997). Sec2p is divided into the N-terminal (residues 1–160) and C-terminal (residues 161–759) regions. The N-terminal region bears the GEF activity on Sec4p (Ortiz et al., 2002), but it lacks sequence similarity to any other GEFs with known structures. On the other hand, the C-terminal region, which lacks conserved structural motifs, does not affect the GEF activity (Elkind et al., 2000; Ortiz et al., 2002), but binds with Sec15p and another RabGTPase, Ypt32p, which recruits Sec2p to the secretory vesicle (Medkova et al., 2006; Ortiz et al., 2002). Thus, on the secretory vesicle, Sec2p activates Sec4p, and the activated Sec4p interacts with Sec15p. Sec15p also interacts with the C-terminal region of Sec2p to displace Ypt32p from Sec2p. In a recent study, Sec2p, Sec4p, and Sec15p were reported to directly interact with each other, which is crucial for Sec2p localization and polarized cellular growth (Medkova et al., 2006).

Mammalian orthologs of Sec4p are Rab3A and Rab8: Rab8 is involved in the transport of Rab8-specific vesicles to the cell surface (Hattula and Peranen, 2000), while

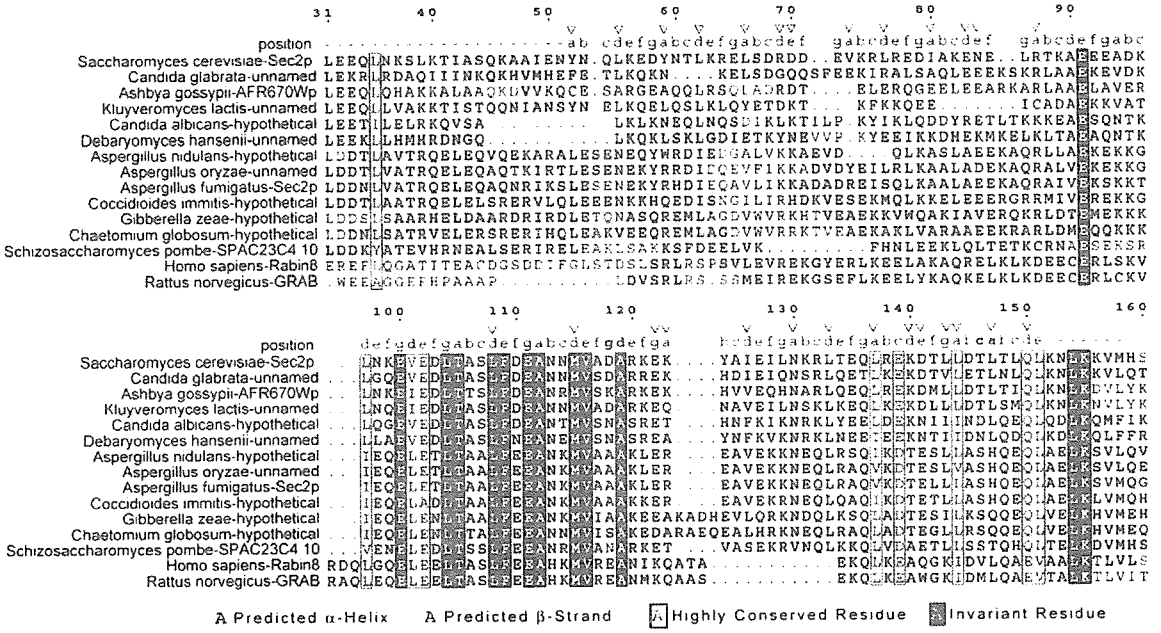

Figure 1. Primary Sequence Alignment of the GEF Domain of Sec2p

The residue numbers and the positions of the coiled-coil heptad repeat of Sec2p are indicated above the sequence alignment. The stutter and stammer are highlighted as red characters. Residues involved in the dimerization of Sec2p are marked with green triangles. Predicted α-helical and β-stranded regions are shown in cyan and yellow, respectively. The highly conserved residues are represented by red characters, while the invariant residues are represented by white characters in a red background. Drawings were made with ESPript (http://espript.ibcp.fr/ESPript/ESPript/index.php).

Rab3A is expressed only in neurons, where it regulates neurotransmitter release (Takai et al., 1996, 2001). The GEFs of Rab8 and Rab3A were identified as Rabin8 (Hattula et al., 2002) and GRAB (Luo et al., 2001), respectively. These mammalian GEFs share the N-terminal region of Sec2p, and have been predicted to have a shorter helical region than that of Sec2p (Figure 1). On the other hand, the C-terminal domain of Sec2p is not conserved in Rabin8 and GRAB, while the C-terminal domain of Rabin8 is essential for its localization and for polarized cellular growth (Hattula et al., 2002), as that of Sec2p, and shares sequence homology with that of GRAB.

To elucidate the mechanism of the nucleotide exchange reaction on Sec4p by Sec2p, we determined the crystal structure of the GEF domain of *S. cerevisiae* Sec2p at 3.0 Å resolution. The structure unexpectedly folds into a parallel dimeric coiled coil, which extends over 180 Å. Biochemical analyses of Sec2p mutants, combined with a docking analysis of Sec2p and Sec4p, uncovered how the simple coiled-coil structure achieves the GEF activity for Rab GTPase.

RESULTS AND DISCUSSION

Sec2p GEF Domain

The N-terminal region of Sec2p (residues 1–160) reportedly has full GEF activity with Sec4p (Ortiz et al., 2002). On the other hand, deletion of the N-terminal 30 residues abolished the GEF activity with Sec4p, while this deletion did not affect the dimerization of Sec2p (Rahl et al., 2005). However, a sequence alignment among Sec2p and its mammalian orthologs, Rabin8 and GRAB, revealed low sequence conservation in the N-terminal 30 residues of Sec2p, which suggests that residues 1–30 of Sec2p are not necessary for the GEF activity. To assess this possibility, we performed in vitro binding and GEF activity assays using $Sec2_{31-160}p$. The results clearly showed that $Sec2_{31-160}p$ can bind to the nucleotide-free Sec4p and displays the full GEF activity, as $Sec2_{1-160}p$ (Ortiz et al., 2002; Walch-Solimena et al., 1997) (Figure 2).

Structure Determination

To determine the crystal structure of the Sec2p GEF domain, we crystallized the recombinant $Sec2_{31-160}p$ in *Escherichia coli*. The details of the crystallization will be published elsewhere. For phasing by anomalous dispersion with the selenium edge, we prepared selenomethionine-labeled $Sec2_{31-160}p$ crystals. However, the crystals diffracted X-rays only to 4.0 Å resolution and were not suitable for the phase determination. To obtain better crystals, we generated eight Sec2p mutants, by replacing the intrinsic Met115 and by incorporating new Met residues, and analyzed the X-ray diffraction of these crystals. Among the mutants, the triple mutant of $Sec2_{31-160}p$

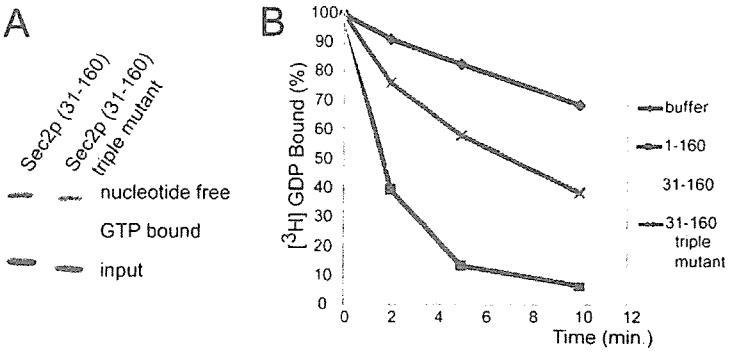

Figure 2. GEF Activity of $Sec2_{31-160}p$
(A) Pull-down assays of GST-Sec4p and Sec2p (wild-type and the triple mutant [Met115Leu, Lys121Met, and Thr142Met]).
(B) [^{3}H]GDP release from GST-Sec4p, in the absence or presence of 30 nM $Sec2_{1-160}p$, $Sec2_{31-160}p$, and $Sec2_{31-160}p$ triple mutant. All of the Sec2p mutants had GEF activity on GST-Sec4p.

(Met115Leu, Lys121Met, and Thr142Met) diffracted X-rays up to 3.0 Å resolution. The crystal structure of this mutant was solved by a single wavelength anomalous dispersion method and was refined to 3.0 Å with 20 molecules (molecules A to T) per asymmetric unit (Figure S1; see the Supplemental Data available with this article online). Several C-terminal residues were structurally disordered. Even in molecules E and F, which are the most ordered in the asymmetric unit, the C-terminal six residues are disordered. While the triple mutation does reduce nucleotide exchange to some degree, its activity is nevertheless similar to that of wild-type (Figure 2). Thus, we concluded here that the structure of this mutant is essentially identical to that of the wild-type.

The Sec2p GEF Domain Forms a Long α-Helical Coiled Coil

As shown in Figure 3, Sec2p folds into a 180 Å long helix and apparently forms a homodimeric, parallel coiled-coil structure, which is similar to that of tropomyosin, a cytoskeleton protein. Coiled coils generally have a heptad repeat sequence labeled "a–g," in which positions "a" and "d" are hydrophobic amino acids, while positions "b," "c," "e," "f," and "g" are hydrophilic ones. Positions "a" and "d" symmetrically face the equivalent residues in the opposite helix, thus forming the core of the coiled coil in a "knobs-into-holes" fashion, while positions "b," "c," "e," "f," and "g" are exposed to the solvent (Lupas, 1996). Some heptad repeats in coiled coils lack three or

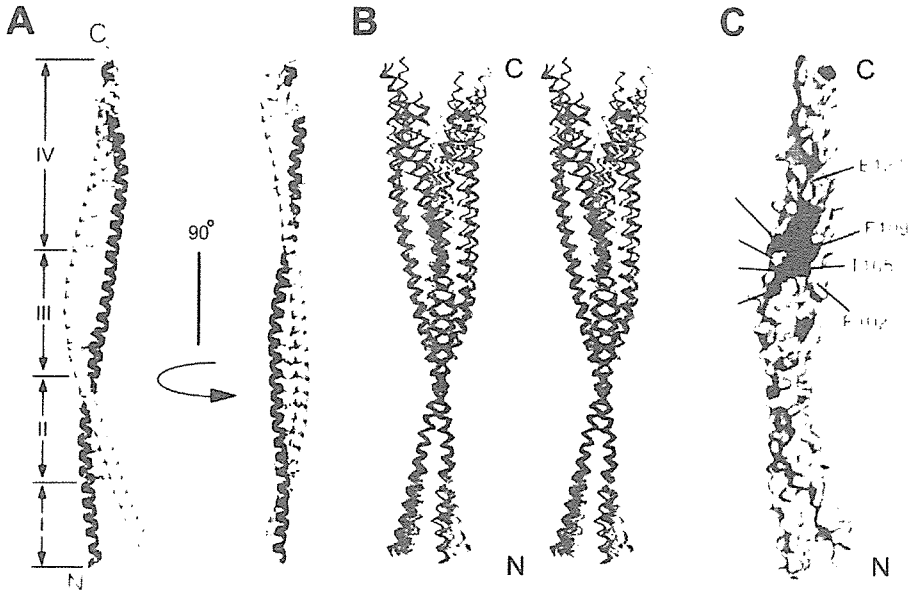

Figure 3. Crystal Structure of the GEF Domain of Sec2p
(A) Ribbon representation of the GEF domain of Sec2p. The side chains that form the core of the coiled coil are colored blue. Based on the heptad repeat sequence and the interhelical distance, the coiled coil is divided into four regions.
(B) Stereo view of the ten coiled coils in the crystallographic asymmetric unit, which are superimposed on region II. Region II is shown in red, and the other regions are color coded for each coiled coil.
(C) Conserved residues, mapped on the Sec2p GEF domain. The orientation is the same as in the left panel of (A). The invariant residues are colored red, while the highly conserved residues are yellow. The labels are colored according to those of the helices in (A).

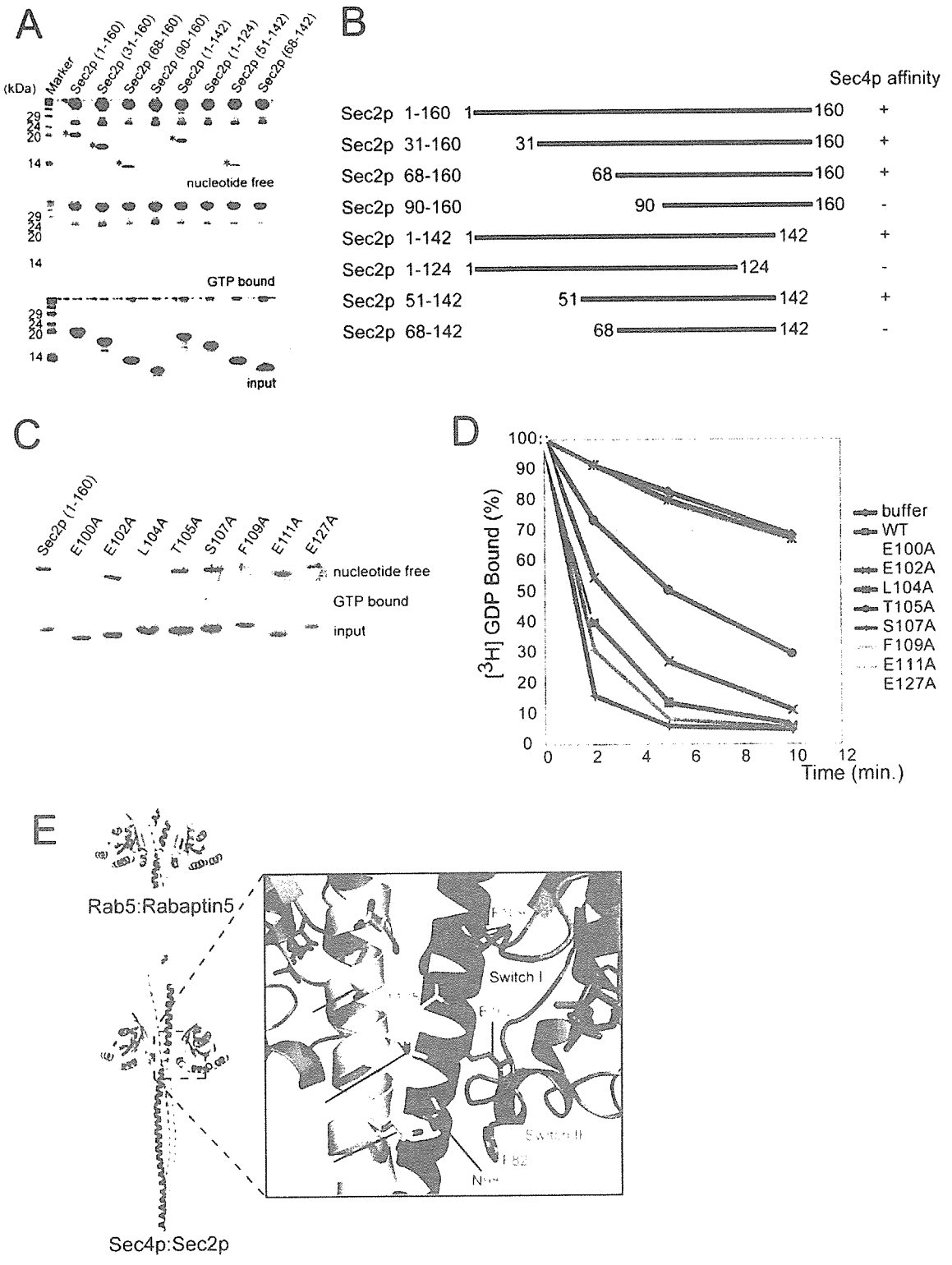
A
(kDa)
Marker
Sec2p (1-160)
Sec2p (31-160)
Sec2p (68-160)
Sec2p (90-160)
Sec2p (1-142)
Sec2p (1-124)
Sec2p (51-142)
Sec2p (68-142)
nucleotide free
GTP bound
input
B
Sec4p affinity
Sec2p 1-160 1 160 +
Sec2p 31-160 31 160 +
Sec2p 68-160 68 160 +
Sec2p 90-160 90 160 -
Sec2p 1-142 1 142 +
Sec2p 1-124 1 124 -
Sec2p 51-142 51 142 +
Sec2p 68-142 68 142 -
C
Sec2p (1-160)
E100A
E102A
L104A
T105A
S107A
F109A
E111A
E127A
nucleotide free
GTP bound
input
D
[3H] GDP Bound (%)
Time (min.)
buffer
WT
E100A
E102A
L104A
T105A
S107A
F109A
E111A
E127A
E
Rab5:Rabaptin5
Switch I
Switch II
Sec4p:Sec2p

four residues, and these are referred to as a "stutter" and a "stammer," respectively (Brown et al., 1996). The heptad repeat sequence and the interhelical distance (i.e., distance between the helical axes) characterize the coiled-coil structure. Here, we divided Sec2p into four regions of residues 31–51 (region I), 52–76 (region II), 77–107 (region III), and 108–150 (region IV), based on the heptad repeat sequence and the interhelical distance (Figure 3 and Figure S2), to clarify the structural properties of the Sec2p coiled coil.

Region I does not form a coiled-coil structure, even though it folds into an α helix (Figure 3). The interhelical distances between the N-terminal edges of the paired coiled coil are 16.3 Å (molecules S and T) and 22.8 Å (molecules C and D). Due to this lack of interhelical contact, the temperature factors are quite high in the N-terminal edge (Figure S2A).

Region II (residues 52–76) contains a normal heptad repeat sequence, with average interhelical distances of 9.8 Å over ten asymmetric coiled-coil molecules (Figure S2A). This value is nearly equal to that of the canonical coiled coil, such as the GCN4 leucine zipper (~9.6 Å on average) (O'Shea et al., 1991). In this region, the Leu55, Leu62, Leu66, Val74, and Leu76 side chains contact the equivalent residues in the opposite helix in a "knobs-into-holes" manner to form the "core" of the coiled coil. The C_β atoms of Tyr52, Tyr59, and Arg69 are also involved in the coiled-coil core formation, while the side chains of these residues protrude toward the solvent.

Region III (residues 77–107) also contains the normal heptad repeat, although there is a "stutter" before Val101 (Figure 1). In this region, the average interhelical distance is 12.6 Å (Figure S2A), which is larger than that of the canonical coiled coil. The Arg87 side chain is oriented toward the opposite helix and thus props the coiled-coil helices apart in this region. As a result, the interhelical space expands in residues 88–107 (Figure 3 and Figure S2A) so that the side chains of Ala90, Ala94, and Val101 are oriented toward the inside of the coiled coil without any interactions, in contrast to the typical rigid coiled coil with a continuous interhelical core. Therefore, $Sec2_{31-160}p$ forms a more flexible and possibly functional coiled coil, especially in region III (Figure 3B).

Region IV (residues 108–150) contains a stutter and a stammer before Ala119 and Leu147, respectively, in the heptad repeat sequence (Figure 1). The interhelical distance is 10.8 Å on average. The side chains of Ala112 and Ala119 (position "a") and Leu108 and Leu115 (position "d") do not correctly face their equivalent residues on the opposite helix but are aligned in a staggered manner (Figure S3). The side chains of Leu108 and Leu115 prop apart the Ala112 and Ala119 side chains. Although Met115 of Sec2p is replaced by Leu115 in our present structure, the wild-type structure should also have the staggered contact in this portion, considering the similar Ala-mediated staggers observed in rat and chicken α-tropomyosin (Figure S3) (Brown et al., 2001, 2005). Residues 120–150 lack the staggered contact, although Asn130, Leu133, Leu144, Leu147, and Gln150 of several coiled-coil molecules asymmetrically contact their equivalent residues in the opposite helix to form the coiled-coil core (data not shown).

The coiled-coil structure of region II (residues 52–76) has two-fold symmetry, whereas those of the other regions are asymmetrical. The coiled-coil structure bends around Ala94: one helix of the coiled coil (molecules B, C, E, H, I, L, M, O, R, and S) bends sharply (13.8° on average, over ten asymmetric coiled-coil molecules), whereas the opposite helix (molecules A, D, F, G, J, K, N, P, Q, and T) bends moderately (8.9° on average) (Figure S2B). The sharply bent helix of residues 108–120 shifts toward the N-terminus by about 2 Å, relative to the opposite moderately bent helix (Figure S3). The aforementioned Ala-mediated stagger and asymmetric contacts are also observed in tropomyosin (Figure S3) and myosin (Brown et al., 2001, 2005) and may contribute to the bending and the functional flexibility of the coiled-coil structure, respectively (Figure 3B, and Figures S2B and S3).

Sec4p Binding Site

To determine how the simple coiled coil of the Sec2p GEF domain binds Sec4p to achieve guanine nucleotide exchange activity, we generated deletion mutants of the Sec2p GEF domain (Figures 4A and 4B) and performed a pull-down binding assay with GST-Sec4p. Since $Sec2_{1-160}p$ interacts with the nucleotide-free Sec4p, but not with the GTP-bound Sec4p (Walch-Solimena et al., 1997), the GTP-bound Sec4p was used as a control for nonspecific binding. In addition, to assess the structural integrity of these deletion mutants, we measured the circular-dichroism (CD) spectra of the mutants, which revealed that the helical contents of $Sec2_{90-160}p$ and $Sec2_{68-142}p$ are lower than those of the other deletion mutants (data not shown). The results of the in vitro binding assays showed that $Sec2_{1-160}p$, $Sec2_{31-160}p$, $Sec2_{68-160}p$, $Sec2_{1-142}p$, and $Sec2_{51-142}p$ can bind with the nucleotide-free Sec4p, but $Sec2_{90-160}p$, $Sec2_{1-124}p$, and $Sec2_{68-142}p$ cannot (Figures 4A and 4B). The binding deficiencies of $Sec2_{90-160}p$ and $Sec2_{68-142}p$ are ascribable to the partially unstructured helices based on the CD spectra analysis. Furthermore, these deletion mutants lack most of the interhelical contact region II (see above), which

Figure 4. In Vitro Sec4p Binding and GEF Activities of Sec2p Mutants

(A) Pull-down assays of GST-Sec4p and truncated mutants of Sec2p. The bound Sec2p mutants are shown by asterisk.

(B) Simplified diagram of (A).

(C) Pull-down assays of GST-Sec4p and point mutants of $Sec2_{1-160}p$.

(D) [^{3}H]GDP release from GST-Sec4p, in the absence or presence of 30 nM wild-type and eight-point mutants of $Sec2_{1-160}p$.

(E) A proposed docking model of GDP-Sec4p (cyan and salmon) and the GEF domain of Sec2p (yellow and green). The Rab5:Rabaptin5 complex structure used to generate the present docking model is presented. The labels and color codes are the same as in Figure 3C.

may result in the disassembly of the coiled-coil dimer. Thus, we concluded that the Sec4p-binding region of Sec2p is located within residues 68–142.

The GEF Active Site Is Formed Across the Dimeric Coiled-Coil Helices

In this anticipated Sec4p binding region of Sec2p (residues 68–142), residues 100–112 are especially conserved among the diverse Sec2p homolog proteins (Brondyk et al., 1995; Hattula et al., 2002; Luo et al., 2001) (Figures 1 and 3C). To identify the Sec4p-binding and catalytic residues of Sec2p, we substituted Ala for the conserved residues that are not involved in the Sec2p dimerization (Figure 1). All of the $Sec2_{1-160}p$ point mutants were well expressed in a soluble form and were tested in in vitro binding assays with GST-Sec4p (Figure 4C). The pull-down assays revealed that the E102A, T105A, S107A, E111A, and E127A $Sec2_{1-160}p$ mutants bound GST-Sec4p as efficiently as the wild-type. In contrast, the E100A mutant was scarcely bound with Sec4p, and the L104A and F109A mutants completely lost their Sec4p-binding activities.

Furthermore, we analyzed the Sec4p GEF activity of these $Sec2_{1-160}p$ mutants by measuring the dissociation of ^3H-labeled GDP from purified GST-Sec4p incubated with the Sec2p mutants (Figure 4D). The E100A, L104A, and F109A mutations abolished the GEF activity on Sec4p, while the E102A and T105A mutants showed moderately reduced GEF activity. Therefore, mutation of Glu102 and Thr105 decreased the Sec4p affinity to some extent, which might adversely affect the nucleotide exchange activity. On the other hand, S107A mutation seems to have significantly increased exchange activity over wild-type. In contrast, the mutations of the other residues (E111A and E127A) had little effect on the GEF activity. Glu100 and Leu104 are clustered with Glu102, Thr105, and Phe109 in the opposite helix, forming a GEF active site lying across the dimeric coiled-coil helices (Figures 3C and 4E). Consistently, the aforementioned deletion analysis suggested that dimer stabilization should be required for the GEF activity.

Docking of Sec2p and Sec4p

Many GTPase-interacting proteins have α-helical motifs, whereas most of the GTPase binding regions lack a parallel coiled coil. To date, only one structure of a coiled coil interacting with a Rab GTPase was reported for the complex between Rab5 and Rabaptin5 effector (Zhu et al., 2004) (Figure 4E). Therefore, we used this complex structure to generate the Sec2p:Sec4p docking model: residues 90–119 of Sec2p were superposed onto residues 807–836 of Rabaptin5, while the crystal structure of GDP-bound Sec4p (Stroupe and Brunger, 2000) was in turn superimposed onto the Rab5 structure with the program CE (Shindyalov and Bourne, 1998). In this docking model, the presently identified Sec4p-binding and catalytic residues (Glu100, Glu102, Leu104, Thr105, and Phe109) approach the Sec4p switch I and II regions. Most GEF proteins interact with the switch regions of their respective small GTPases, which surround the bound guanine nucleotide, and induce conformational changes mainly in the switch I region to release GDP (Boriack-Sjodin et al., 1998; Goldberg, 1998; Itzen et al., 2006; Worthylake et al., 2000). This fact may validate our Sec2p:Sec4p complex model.

These GTPase-binding and catalytic residues are conserved in the mammalian Rab GEFs, Rabin8, and GRAB (Figure 1). Furthermore, the amino acid segment encompassing residues 99–120 of Sec2p, which mostly cover the Sec4p binding region, are completely identical between Rabin8 and GRAB (Figure 1). Despite the sequence identity, the specificity for Rab GTPases differs between Rabin8 and GRAB; Rabin8 exchanges GDP for GTP on Rab8, but not on Rab3A (Hattula et al., 2002), while GRAB exchanges nucleoside on Rab3A (Luo et al., 2001). This Rab GTPase specificity is ascribable to the residue corresponding to Asn98 in Sec2p since Asn98 is the only residue close to Sec4p other than the residues 99–120 in the present docking model. In our docking model, Asn98 approaches Phe82 in the switch II region of Sec4p (Figure 4E). The Sec2p Asn98 is replaced by Gly in Rabin8, while by Glu in GRAB (Figure 1). Consistently, only a difference in the switch II region between Rab3A and Rab8 is the substitution of Phe (Rab8) for Tyr84 (Rab3A) (Figure S4), which promptly corresponds to the Phe82 of Sec2p. Therefore, our docking model may further account for the Rab GTPase specificity by the respective GEF proteins. Clarification of the detailed mechanism underlying the GTPase specificity awaits the structural determination of the Sec2p:Sec4p complex, which is now under way.

Concluding Remarks

To our knowledge, the Sec2p GEF domain is the first to reveal a parallel coiled-coil structure possessing GEF activity on a small GTPase. This apparently simple structure achieves the Sec4p binding and the guanine nucleotide exchange activity on this small GTPase. Based on the present structural and functional analyses, we can speculate that the coiled-coil GEF domain of Sec2p emerged by divergent evolution from an ancestral Rab GTPase effector with a homodimeric, parallel coiled coil.

EXPERIMENTAL PROCEDURES

Structure Determination and Refinement

Site-directed mutations were generated by PCR. The selenomethionine-labeled triple mutant $Sec2_{31-160}p$ (Met115Leu, Lys121Met, and Thr142Met) was crystallized at 20°C by the hanging drop vapor diffusion method against a reservoir solution containing 50 mM Tris•Cl (pH 7.5), 10 mM $MgCl_2$, and 3% isopropanol. For data collection, the crystals were transferred to a cryostabilizing solution (50 mM Tris•Cl [pH 7.5], 10 mM $MgCl_2$, 3.5% isopropanol, and 35% glycerol), and flash frozen in a 100 K nitrogen stream. The diffraction data set was collected at the beamline BL5A at the Photon Factory (Tsukuba, Japan). Data were processed with the programs Denzo and Scalepack (Otwinowski and Minor, 1997). The structure was solved by single-wavelength anomalous dispersion. At first, the crystal apparently belonged to the space group $P2_12_12_1$, with unit cell dimensions a = 101.93 Å, b = 176.56 Å, c = 181.45 Å. Ten of the 20 possible selenium sites were identified by the program SnB (Weeks and Miller, 1999). Refinement

Table 1. Data Collection, Phasing, and Refinement Statistics

	SeMet
Data Collection	
X-ray source	PF BL5A
Wavelength (Å)	0.97934
Resolution (Å)	50.0–3.0 (3.11–3.00)
Unique reflections	65,695
Total reflections	655,703
Completeness	99.3 (98.2)
$I/\sigma(I)$	29.2 (2.2)
R_{sym}	0.080 (0.422)
Phasing Statistics	
Number of sites	10
Phasing power	
Anomalous (acentrics)	0.669
R_{cullis}	
Anomalous (acentrics)	0.895
Mean overall figure of merit	
Acentric	0.15577
Centric	0.02503
After density modification	0.796
Refinement Statistics	
Number of atoms: protein, water	19,028, 262
Luzzati coordinate error (Å)	0.39
Crossvalidated Luzzati coordinate error (Å)	0.46
Rmsd bond length (Å)	0.010
Rmsd bond angle (°)	1.3
Rmsd dihedral angle (°)	19
Rmsd improper angle (°)	0.61
B factors: minimum, average, maximum (Å^2)	3.1, 138.1, 202.1
Residues in core region (%)	89.4
Residues in additionally allowed region (%)	10.6
Residues in generously allowed region (%)	0.0
Residues in disallowed region (%)	0.0
R_{work}, R_{free} [a]	0.229, 0.285

[a] 7.5% of the total unique reflections were randomly selected for the R_{free} calculation.

of the selenium sites and phase calculation were carried out with the program SHARP (De La Fortelle and Bricogne, 1997). Subsequent phase improvement by solvent flipping was carried out with the program Solomon (Abrahams and Leslie, 1996). The atomic model was built with the program O (Jones et al., 1991). The model was refined up to 3.0 Å resolution with the program CNS (Brunger et al., 1998) against the data processed with $P2_12_12_1$, but the R_{free} value was not improved, and the resultant $2F_o - F_c$ map became worse than the experimental map. We therefore suspected pseudosymmetry and expanded the data from the $P2_12_12_1$ space group to $P2_1$. This assisted the refinement procedure, but the R_{free} value was still around 35%. Finally, we suspected pseudomerohedral perfect twinning. The introduction of the twinning parameter to the refinement markedly improved the R_{free} values and the electron density map. Data collection, phasing, and refinement statistics are shown in Table 1. All molecular graphics were prepared with the program PyMOL (http://pymol.sourceforge.net/).

In Vitro Binding Assay

For the nucleotide-free Sec4p, GST-Sec4p, immobilized on glutathione-Sepharose beads, was incubated with 10 mM EDTA, 50 mM Tris•Cl (pH 7.2), 100 mM NaCl, and 1 mM DTT for 90 min at room temperature and then was incubated with the Sec2p mutants, in 50 mM Tris•Cl (pH 7.2), 100 mM NaCl, and 1 mM DTT. For the GTP-bound Sec4p, GST-Sec4p, immobilized on glutathione-Sepharose beads, was incubated with 1 mM GTP, 10 mM EDTA, 50 mM Tris•Cl (pH 7.2), 100 mM NaCl, and 1 mM DTT for 90 min at room temperature, and the reaction was terminated by adding 10 mM $MgCl_2$. The GTP-bound GST-Sec4p was then incubated with several Sec2p mutants, in 1 mM GTP, 10 mM MgCl2, 50 mM Tris•Cl (pH 7.2), 100 mM NaCl, and 1 mM DTT. The proteins bound to the beads were released by boiling in SDS loading buffer, analyzed by SDS-PAGE, and stained with Coomassie brilliant blue.

Nucleotide Exchange Assays

GST-Sec4p (2 μM) was preloaded with [^{3}H]GDP, by an incubation in 50 mM HEPES-KOH (pH 7.4), 100 mM NaCl, 5 mM $MgCl_2$, 1 mM DTT, 10 mM EDTA, 10 μM GDP, and [^{3}H]GDP for 15 min at 30°C. After the incubation, 10 mM $MgCl_2$ and 2 mM GTP were added, and the solution was placed on ice to stop the reaction. Reactions were initiated by the addition of 10 μl of 30 nM purified Sec2p or control buffer (50 mM HEPES-KOH [pH 7.4], 100 mM NaCl, 5 mM $MgCl_2$, and 1 mM DTT) to 10 μl of [^{3}H]GDP preloaded GST-Sec4p. To reduce the intrinsically high GDP release from GST-Sec4p, the reactions were conducted at 16°C. The reactions were stopped by adding 800 μl of ice-cold 50 mM HEPES-KOH (pH 7.4), 100 mM NaCl, 5 mM $MgCl_2$, and 1 mM DTT. The Sec4p-retained radioactivity was monitored by filter binding, followed by scintillation counting.

Supplemental Data

Supplemental Data include figures and legends and are available at http://www.structure.org/cgi/content/full/15/2/245/DC1/.

ACKNOWLEDGMENTS

We thank the beamline staffs at BL5A of PF (Tsukuba, Japan) for technical help during data collection. This work was supported by a SORST Program grant from JST (Japan Science and Technology) to O.N., by a grant for the National Project on Protein Structural and Functional Analyses from the Ministry of Education, Culture, Sports, Science and Technology (MEXT) to O.N. and S.F., by grants from MEXT to O.N. and S.F., and by Kurata Memorial Hitachi Science and Technology Foundation grants to S.F.

Received: January 11, 2007
Revised: January 11, 2007
Accepted: January 11, 2007
Published: February 13, 2007

REFERENCES

Abrahams, J.P., and Leslie, A.G.W. (1996). Methods used in the structure determination of bovine mitochondrial F1 ATPase. Acta Crystallogr. D Biol. Crystallogr. *52*, 429–439.

Boriack-Sjodin, P.A., Margarit, S.M., Bar-Sagi, D., and Kuriyan, J. (1998). The structural basis of the activation of Ras by Sos. Nature *394*, 337–343.

Brondyk, W.H., McKiernan, C.J., Fortner, K.A., Stabila, P., Holz, R.W., and Macara, I.G. (1995). Interaction cloning of Rabin3, a novel protein that associates with the Ras-like GTPase Rab3A. Mol. Cell. Biol. *15*, 1137–1143.

Brown, J.H., Cohen, C., and Parry, D.A. (1996). Heptad breaks in alpha-helical coiled coils: stutters and stammers. Proteins *26*, 134–145.

Brown, J.H., Kim, K.H., Jun, G., Greenfield, N.J., Dominguez, R., Volkmann, N., Hitchcock-DeGregori, S.E., and Cohen, C. (2001). Deciphering the design of the tropomyosin molecule. Proc. Natl. Acad. Sci. USA *98*, 8496–8501.

Brown, J.H., Zhou, Z., Reshetnikova, L., Robinson, H., Yammani, R.D., Tobacman, L.S., and Cohen, C. (2005). Structure of the mid-region of tropomyosin: bending and binding sites for actin. Proc. Natl. Acad. Sci. USA *102*, 18878–18883.

Brunger, A.T., Adams, P.D., Clore, G.M., DeLano, W.L., Gros, P., Grosse-Kunstleve, R.W., Jiang, J.S., Kuszewski, J., Nilges, M., Pannu, N.S., et al. (1998). Crystallography & NMR system: a new software suite for macromolecular structure determination. Acta Crystallogr. D Biol. Crystallogr. *54*, 905–921.

Elkind, N.B., Walch-Solimena, C., and Novick, P.J. (2000). The role of the COOH terminus of Sec2p in the transport of post-Golgi vesicles. J. Cell Biol. *149*, 95–110.

De La Fortelle, E., and Bricogne, G. (1997). Maximum-likelihood heavy-atom parameter refinement for multiple isomorphous replacement and multiwavelength anomalous diffraction methods. Methods Enzymol. *276*, 472–494.

Goldberg, J. (1998). Structural basis for activation of ARF GTPase: mechanisms of guanine nucleotide exchange and GTP-myristoyl switching. Cell *95*, 237–248.

Guo, W., Roth, D., Walch-Solimena, C., and Novick, P. (1999). The exocyst is an effector for Sec4p, targeting secretory vesicles to sites of exocytosis. EMBO J. *18*, 1071–1080.

Hattula, K., and Peranen, J. (2000). FIP-2, a coiled-coil protein, links Huntingtin to Rab8 and modulates cellular morphogenesis. Curr. Biol. *10*, 1603–1606.

Hattula, K., Furuhjelm, J., Arffman, A., and Peranen, J. (2002). A Rab8-specific GDP/GTP exchange factor is involved in actin remodeling and polarized membrane transport. Mol. Biol. Cell *13*, 3268–3280.

Itzen, A., Pylypenko, O., Goody, R.S., Alexandrov, K., and Rak, A. (2006). Nucleotide exchange via local protein unfolding–structure of Rab8 in complex with MSS4. EMBO J. *25*, 1445–1455.

Jones, T.A., Zou, J.Y., Cowan, S.W., and Kjeldgaard, M. (1991). Improved methods for binding protein models in electron density maps and the location of errors in these models. Acta Crystallogr. A *47*, 110–119.

Lipschutz, J.H., and Mostov, K.E. (2002). Exocytosis: the many masters of the exocyst. Curr. Biol. *12*, R212–R214.

Luo, H.R., Saiardi, A., Nagata, E., Ye, K., Yu, H., Jung, T.S., Luo, X., Jain, S., Sawa, A., and Snyder, S.H. (2001). GRAB: a physiologic guanine nucleotide exchange factor for Rab3A, which interacts with inositol hexakisphosphate kinase. Neuron *31*, 439–451.

Lupas, A. (1996). Coiled coils: new structures and new functions. Trends Biochem. Sci. *21*, 375–382.

Medkova, M., France, Y.E., Coleman, J., and Novick, P. (2006). The rab exchange factor Sec2p reversibly associates with the exocyst. Mol. Biol. Cell *17*, 2757–2769.

O'Shea, E.K., Klemm, J.D., Kim, P.S., and Alber, T. (1991). X-ray structure of the GCN4 leucine zipper, a two-stranded, parallel coiled coil. Science *254*, 539–544.

Ortiz, D., Medkova, M., Walch-Solimena, C., and Novick, P. (2002). Ypt32 recruits the Sec4p guanine nucleotide exchange factor, Sec2p, to secretory vesicles; evidence for a Rab cascade in yeast. J. Cell Biol. *157*, 1005–1015.

Otwinowski, Z., and Minor, W. (1997). Processing of X-ray diffraction data collected in oscillation mode. Methods Enzymol. *276*, 307–326.

Rahl, P.B., Chen, C.Z., and Collins, R.N. (2005). Elp1p, the yeast homolog of the FD disease syndrome protein, negatively regulates exocytosis independently of transcriptional elongation. Mol. Cell *17*, 841–853.

Shindyalov, I.N., and Bourne, P.E. (1998). Protein structure alignment by incremental combinatorial extension (CE) of the optimal path. Protein Eng. *11*, 739–747.

Stroupe, C., and Brunger, A.T. (2000). Crystal structures of a Rab protein in its inactive and active conformations. J. Mol. Biol. *304*, 585–598.

Takai, Y., Sasaki, T., Shirataki, H., and Nakanishi, H. (1996). Rab3A small GTP-binding protein in Ca(2+)-dependent exocytosis. Genes Cells *1*, 615–632.

Takai, Y., Sasaki, T., and Matozaki, T. (2001). Small GTP-binding proteins. Physiol. Rev. *81*, 153–208.

TerBush, D.R., Maurice, T., Roth, D., and Novick, P. (1996). The Exocyst is a multiprotein complex required for exocytosis in *Saccharomyces cerevisiae*. EMBO J. *15*, 6483–6494.

Walch-Solimena, C., Collins, R.N., and Novick, P.J. (1997). Sec2p mediates nucleotide exchange on Sec4p and is involved in polarized delivery of post-Golgi vesicles. J. Cell Biol. *137*, 1495–1509.

Weeks, C.M., and Miller, R. (1999). The design and implementation of SnB v2.0. J. Appl. Cryst. *32*, 120–124.

Worthylake, D.K., Rossman, K.L., and Sondek, J. (2000). Crystal structure of Rac1 in complex with the guanine nucleotide exchange region of Tiam1. Nature *408*, 682–688.

Zhu, G., Zhai, P., Liu, J., Terzyan, S., Li, G., and Zhang, X.C. (2004). Structural basis of Rab5-Rabaptin5 interaction in endocytosis. Nat. Struct. Mol. Biol. *11*, 975–983.

Accession Numbers

The atomic coordinates have been deposited in the Protein Data Bank, http://www.rcsb.org/ (PDB ID code 2E7S).

J Appl Physiol 102: 1007–1013, 2007.
First published November 22, 2006; doi:10.1152/japplphysiol.01034.2006.

Effect of acute activation of 5′-AMP-activated protein kinase on glycogen regulation in isolated rat skeletal muscle

Licht Miyamoto,[1] Taro Toyoda,[2] Tatsuya Hayashi,[1,3] Shin Yonemitsu,[1] Masako Nakano,[1] Satsuki Tanaka,[1] Ken Ebihara,[1] Hiroaki Masuzaki,[1] Kiminori Hosoda,[1] Yoshihiro Ogawa,[1] Gen Inoue,[1] Tohru Fushiki,[2] and Kazuwa Nakao[1]

[1]*Department of Medicine and Clinical Science, Graduate School of Medicine,* [2]*Laboratory of Nutrition Chemistry, Division of Food Science and Biotechnology, Graduate School of Agriculture, and* [3]*Laboratory of Sports and Exercise Medicine, Graduate School of Human and Environmental Studies, Kyoto University, Kyoto, Japan*

Submitted 15 September 2006; accepted in final form 19 November 2006

Miyamoto L, Toyoda T, Hayashi T, Yonemitsu S, Nakano M, Tanaka S, Ebihara K, Masuzaki H, Hosoda K, Ogawa Y, Inoue G, Fushiki T, Nakao K. Effect of acute activation of 5′-AMP-activated protein kinase on glycogen regulation in isolated rat skeletal muscle. *J Appl Physiol* 102: 1007–1013, 2007. First published November 22, 2006; doi:10.1152/japplphysiol.01034.2006.—5′-AMP-activated protein kinase (AMPK) has been implicated in glycogen metabolism in skeletal muscle. However, the physiological relevance of increased AMPK activity during exercise has not been fully clarified. This study was performed to determine the direct effects of acute AMPK activation on muscle glycogen regulation. For this purpose, we used an isolated rat muscle preparation and pharmacologically activated AMPK with 5-aminoimidazole-4-carboxamide-1-β-D-ribonucleoside (AICAR). Tetanic contraction in vitro markedly activated the α_1- and α_2-isoforms of AMPK, with a corresponding increase in the rate of 3-*O*-methylglucose uptake. Incubation with AICAR elicited similar enhancement of AMPK activity and 3-*O*-methylglucose uptake in rat epitrochlearis muscle. In contrast, whereas contraction stimulated glycogen synthase (GS), AICAR treatment decreased GS activity. Insulin-stimulated GS activity also decreased after AICAR treatment. Whereas contraction activated glycogen phosphorylase (GP), AICAR did not alter GP activity. The muscle glycogen content decreased in response to contraction but was unchanged by AICAR. Lactate release was markedly increased when muscles were stimulated with AICAR in buffer containing glucose, indicating that the glucose taken up into the muscle was catabolized via glycolysis. Our results suggest that AMPK does not mediate contraction-stimulated glycogen synthesis or glycogenolysis in skeletal muscle and also that acute AMPK activation leads to an increased glycolytic flux by antagonizing contraction-stimulated glycogen synthesis.

contraction; glycogen synthase; glycogen phosphorylase; epitrochlearis muscle; glycolysis

EXERCISE PROFOUNDLY AFFECTS glycogen metabolism by stimulating glycogenolysis during exercise, which is followed by the resynthesis of glycogen after exercise. Intracellular glycogen plays a major role as a fuel for acute muscle contraction, and its concentration is dramatically reduced in response to a single bout of exercise (6, 14, 25, 38). The facilitation of glycogen resynthesis after exercise causes a marked accumulation of glycogen, i.e., the well-known phenomenon of glycogen supercompensation. Similar to exercise, insulin causes strong glucose uptake and glycogen synthesis. Therefore, the increase in insulin sensitivity in skeletal muscle after exercise also plays an important role in glucose metabolism (11, 25, 36). In contrast to the physiological relevance of muscle glycogen, the signaling mechanisms leading to the regulation of glycogen synthesis and glycogenolysis in contracting muscle have not been fully clarified.

Several aspects of the contraction-evoked metabolic events in skeletal muscle have been shown to be related to 5′-AMP-activated protein kinase (AMPK), including GLUT4 translocation and glucose transport (1, 4, 18, 19, 27, 31, 32), fatty acid oxidation via the inactivation of acetyl-CoA carboxylase (23, 32, 41, 43), GLUT4 expression (7, 21, 22, 32, 35, 44, 48), and insulin sensitivity (12, 24, 32). AMPK, a heterotrimeric serine/threonine protein kinase, consists of a catalytic α-subunit and regulatory β- and γ-subunits. Two distinct α-isoforms, α_1 and α_2, are expressed in skeletal muscle (39), and both isoforms can be activated in response to muscle contraction (40). AMPK is allosterically activated in response to an elevation in AMP concentration or in the AMP-to-ATP ratio. It is also activated when phosphorylated by upstream kinases (42, 46). Therefore, it has been hypothesized that AMPK acts as an intracellular energy sensor that plays a key role in regulating cellular metabolism in skeletal muscle (9, 13, 18, 19, 23, 37, 41, 43).

Recent studies of natural and manipulated mutations in AMPK suggest that chronic changes in AMPK action have substantial effects on glycogen metabolism in skeletal muscle. The glycogen concentration in the gastrocnemius muscles of mice that muscle-specifically express a dominant-negative kinase-dead form of the α-isoform is about half that observed in nontransgenic mice (31), although glycogen synthase (GS) activity and glycogen phosphorylase (GP) activity are not significantly different between the transgenic and nontransgenic animals under basal conditions or after contraction (30). The AMPK R225Q mutation in the *PRKAG3* gene, which encodes the muscle-specific isoform of the γ_3-subunit of AMPK, leads to increased glycogen accumulation in Hampshire pig skeletal muscle (29). The amount of glycogen in the gastrocnemius muscle is twofold higher in the R225Q *PRKAG3* transgenic mouse than in the wild-type mouse but is unaltered in the *PRKAG3*-null mouse (5). In contrast, another mutation has been identified in the pig *PRKAG3* gene (V224I) that is associated with low muscle glycogen (10). It has also been suggested that mutations in *PRKAG2*, the gene for the γ_2-subunit of AMPK, cause glycogen-associated vacuoles to

Address for reprint requests and other correspondence: T. Hayashi, Laboratory of Sports and Exercise Medicine, Graduate School of Human and Environmental Studies, Kyoto Univ., Yoshida-nihonmatsu-cho, Sakyo-ku, Kyoto 606-8501, Japan (e-mail: tatsuya@kuhp.kyoto-u.ac.jp).

The costs of publication of this article were defrayed in part by the payment of page charges. The article must therefore be hereby marked "*advertisement*" in accordance with 18 U.S.C. Section 1734 solely to indicate this fact.

form in myocytes, leading to a glycogen storage disease of the cardiac muscle (2).

The physiological relevance of the acute elevation of AMPK activity during exercise to muscle glycogen regulation has not been fully elucidated. Halse et al. (16) reported GS inactivation in accordance with AMPK activation after 2 h of glucose starvation in the medium in human myoblast cells in culture. They also showed that stimulation by 5-aminoimidazole-4-carboxamide-1-β-D-ribonucleoside (AICAR) or hydrogen peroxide caused AMPK activation and concurrent GS inactivation. Wojtaszewski et al. (45) demonstrated that the addition of AICAR to the circulation medium resulted in increased AMPK-α_2 activity and decreased GS activity in perfused rat skeletal muscles. AICAR is taken up into muscle cells and metabolized to form ZMP, a monophosphorylated derivative that mimics the stimulatory effects of AMP on AMPK without changing the concentration of AMP or ATP (17). In fact, GS Ser^7 can be phosphorylated and inactivated by AMPK in vitro (8) and in vivo (26). Wojtaszewski et al. also found significant activation of α_2-AMPK and inactivation of GS when muscle glycogen was depleted by prolonged exercise and restricted diet. In contrast, repeated activation of AMPK by the administration of AICAR for 5–28 days increased glycogen concentration in rat skeletal muscles (7, 21, 44). Aschenbach et al. (3) demonstrated acute activation of AMPK-α_2 in red and white gastrocnemius muscles in normal rats after a single intraperitoneal dose of AICAR. However, GS activity was reduced only in white gastrocnemius muscle, whereas GS activity conversely increased in red gastrocnemius muscle (3). They also made the contradictory observation that in vitro incubation with AICAR had no effect on GS activity in isolated rat muscles (epitrochlearis or flexor digitorum brevis) (3).

Therefore, we undertook the present study to elucidate the direct effects of acute AMPK activation, which is comparable to activation in contracting muscle on glycogenolysis and glycogen synthesis in mature skeletal muscle. For this purpose, we used an isolated rat muscle preparation and pharmacologically manipulated muscle AMPK with AICAR stimulation, which allowed us to activate AMPK-α_1 and -α_2 to a level similar to that observed after tetanic contraction in skeletal muscle. We demonstrate that activation of AMPK, in contrast to muscle contraction, does not cause GS or GP activation, nor does it cause a decrease in muscle glycogen. We propose that AMPK activation per se antagonizes glycogen synthesis in contracting muscle and facilitates the regeneration of ATP via glycolysis.

MATERIALS AND METHODS

Materials. All radioactive materials ([γ-^{32}P]ATP, 3-*O*-methyl-[^{3}H]glucose, [^{14}C]mannitol, [^{14}C]UDP-glucose, and [^{14}C]glucose 1-phosphate) were obtained from Perkin Elmer Japan (Yokohama, Japan), human insulin (Humulin R) from Eli Lilly (Indianapolis, IN), P81 filter paper from Whatman (Brentford, UK), and protein A-Sepharose from GE Healthcare Bioscience (Little Chalfont, UK). All other reagents were of analytic grade and were obtained from Sigma-Aldrich (St. Louis, MO), unless otherwise stated.

Animals. Male Sprague-Dawley rats (120–130 g body wt; Japan SLC, Hamamatsu, Japan) were housed in an animal facility maintained at 20°C with a 12:12-h light-dark cycle and allowed free access to water and standard rodent chow. After an overnight fast, the rats were randomly assigned to experimental groups. The Kyoto University Graduate School of Medicine Committee on Animal Research approved all experimental procedures.

Muscle sample preparation. Animals were killed by cervical dislocation. The epitrochlearis muscles were rapidly isolated and incubated as previously described (19), with some modifications. Briefly, the muscles were preincubated for 40 min in 6 ml of Krebs-Ringer bicarbonate (KRB) buffer, pH 7.4, containing 2 mM sodium pyruvate (KRB-P). For the dose-response and time-course changes in AICAR-stimulated AMPK activity, muscles were incubated in the absence or presence of AICAR (0.03, 0.125, 0.5, 2, or 8 mM) for 40 min or in the presence of 2 mM AICAR for 10, 30, 40, or 60 min, respectively. On the basis of these experiments, we decided to stimulate muscles with 2 mM AICAR for 40 min in other experiments (see RESULTS). For insulin treatment, muscles were preincubated and then incubated in the presence of 1 μM insulin for 40 min. For epinephrine treatment, muscles were preincubated and then incubated in the presence of 3 μg/ml epinephrine for the last 15 min of the incubation period (total 40 min). Muscle contractions were induced by preincubation of muscles and then incubation in KRB-P for 40 min, followed by electrical stimulation during the last 10 min, as described previously (19) (1/min train rate, 10-s train duration, 100-Hz pulse rate, 0.1-ms pulse duration, 100 V). The buffers were continuously gassed with 95% O_2-5% CO_2 and maintained at 37°C. The muscles were then used for glucose uptake measurements (see *Glucose uptake*) or trimmed and immediately frozen in liquid nitrogen for other assays. For the measurement of lactate release, we used KRB containing 8 mM glucose during preincubation and stimulation. AICAR treatment and muscle contractions were performed as described above.

Isoform-specific AMPK activity. AMPK activity was determined as described previously, with slight modifications (40). Frozen muscles were homogenized in ice-cold lysis buffer (1:60, wt/vol) containing 20 mM HEPES (pH 7.4), 1% Triton X-100, 50 mM sodium chloride, 50 mM sodium fluoride, 5 mM sodium pyrophosphate, 2 mM dithiothreitol, 4 mg/l leupeptin, 50 mg/l trypsin inhibitor, 0.1 mM benzamidine, and 0.5 mM phenylmethylsulfonyl fluoride and then centrifuged at 14,000 *g* for 20 min at 4°C. The supernatants (200 μg of protein) were immunoprecipitated with isoform-specific antibodies directed against the α_1- or α_2-subunit of AMPK (40) and protein A-Sepharose beads. The immune complex was washed extensively with 240 mM HEPES (pH 7.0) and 480 mM sodium chloride. Kinase activity was determined by the phosphorylation of the SAMS peptide (40). The kinase reaction was carried out in 40 mM HEPES (pH 7.0), 0.1 mM SAMS, 0.2 mM AMP, 80 mM sodium chloride, 0.8 mM dithiothreitol, 5 mM magnesium chloride, and 0.2 mM ATP (2 μCi of [γ-^{32}P]ATP) for 20 min at 30°C. The reaction products were then spotted onto P81 filter papers, which were extensively washed in 1% phosphoric acid, and the radioactivity on the dried papers was quantified with a liquid scintillation counter (Aloka, Tokyo, Japan).

Glucose uptake. We evaluated 3-*O*-methylglucose (3-MG) uptake as an index of glucose uptake activity. 3-MG uptake was determined as described previously (19), with modifications. After the incubation period, muscles were incubated in KRB containing 1 mM 3-MG, 1.5 μCi/ml [^{3}H]3-MG, 7 mM mannitol, and 0.3 μCi/ml [^{14}C]mannitol at 30°C for 10 min. The muscles were then trimmed and frozen in liquid nitrogen. The muscles were processed by incubation in 1 M NaOH at 85°C for 10 min, and the digestates were neutralized with HCl. The radioactivity in aliquots of the digestates was determined by liquid scintillation counting of dual labels, and the extracellular and intracellular spaces were calculated. The rate of 3-MG uptake was expressed as micromoles of 3-MG per milliliter of intracellular space per hour.

GS activity. GS activity was determined as described previously (19), with modifications. Frozen muscles were homogenized in lysis buffer (*buffer A*) containing 20 mM HEPES (pH 7.4), 1% Triton X-100, 50 mM sodium chloride, 50 mM sodium fluoride, 5 mM sodium pyrophosphate, 2 mM EGTA, 50 mM β-glycerophosphate, 4 mg/l leupeptin, 10 μg/ml aprotinin, 3 mM benzamidine, and 0.5 mM